arXiv:astro-ph/0305228v1 13 May 2003

THE 160 SQUARE DEGREE *ROSAT* SURVEY: THE REVISED CATALOG OF 201 CLUSTERS WITH SPECTROSCOPIC REDSHIFTS[1]

C.R. Mullis[2,3], B.R. McNamara[4,5], H. Quintana[6], A. Vikhlinin[5], J.P. Henry[3], I.M. Gioia[7,3], A. Hornstrup[8], W. Forman[5], and C. Jones[5]

Accepted for publication in ApJ

ABSTRACT

We present the revised catalog of galaxy clusters detected as extended X-ray sources in the 160 Square Degree *ROSAT* Survey, including spectroscopic redshifts and X-ray luminosities for 200 of the 201 members. The median redshift is $z_{\rm median} = 0.25$ and the median X-ray luminosity is $L_{\rm X,median} = 4.2{\times}10^{43}$ h_{50}^{-2} erg s^{-1} (0.5–2.0 keV). This is the largest high-redshift sample of X-ray selected clusters published to date. There are 73 objects at $z > 0.3$ and 22 objects at $z > 0.5$ drawn from a statistically complete flux-limited survey with a median object flux of 1.4×10^{-13} erg cm^{-2} s^{-1}. We describe the optical follow-up of these clusters with an emphasis on our spectroscopy which has yielded 155 cluster redshifts, 110 of which are presented here for the first time. These measurements combined with 45 from the literature and other sources provide near-complete spectroscopic coverage for our survey. We discuss the final optical identifications for the extended X-ray sources in the survey region and compare our results to similar X-ray cluster searches.

Subject headings: catalogs — galaxies: clusters: general — surveys — X-rays: galaxies

1. INTRODUCTION

According to the theory of hierarchical structure formation, clusters of galaxies are amongst the largest and most recent systems to form in the matrix of cosmic construction (e.g., Peebles 1993; Peacock 1999). Measurements based on dynamical, gravitational lensing, and X-ray data independently confirm the extreme magnitude of cluster masses (10^{14}–10^{15} $M_\odot$); thus situating them as the largest virialized masses in the Universe (e.g., Smail et al. 1997; Wu et al. 1998; Allen et al. 2001; Clowe & Schneider 2002). Observed phenomena including cluster-cluster mergers, shock fronts, infalling sub-clusters, and non-spherical morphologies attest to the on-going assembly of clusters. (e.g., Gioia et al. 1999; Vikhlinin, Markevitch, & Murray 2001; Czoske et al. 2002; Markevitch et al. 2002; Rose et al. 2002).

As galaxy clusters form in the deepest gravitational potentials, presumably at the intersections of filaments in the "cosmic web" of large-scale structure, they are excellent tracers of the matter distribution in the Universe (e.g., Bond, Kofman, & Pogosyan 1996; Jenkins et al. 1998; Mullis et al. 2001; Borgani & Guzzo 2001). Moreover, clusters are important tools for constraining cosmological parameters. For example, determinations of the mass, X-ray luminosity, and X-ray temperature functions can be used to measure the matter density parameter (Ω_M) and the amplitude (σ_8) of density fluctuations (e.g., Henry 2000; Borgani et al. 2001; Vikhlinin et al. 2003). Observations of the Sunyaev-Zeldovich (SZ) effect combined with X-ray imaging of clusters can be used to assess the Hubble parameter (H_0) via a technique notably independent of the distance ladder (e.g., Sunyaev & Zeldovich 1972; Silk & White 1978; Carlstrom, Holder, & Reese 2002;). By no means is this overview of systemic cluster applications complete; see the reviews, and references therein, of Sarazin (1988) for a historical perspective on cluster X-ray emission, Mulchaey (2000) for the X-ray properties of galaxy groups, and Rosati, Borgani, & Norman (2002) for the current understanding of evolutionary trends in X-ray clusters of galaxies.

The significance of galaxy clusters and the strong interest to discover and investigate these remarkable structures are demonstrated by the sheer number of surveys undertaken in recent years. In the high-energy domain alone, there are at least sixteen independent X-ray-selected cluster surveys spanning the *Einstein* and *ROSAT* eras (see Table 1). X-ray selection is currently the optimal procedure for building cluster samples with minimum bias and maximum statistical completeness. Techniques currently under development that may offer a competitive alternative include gravitational lensing and SZ surveys. Rosati et al. (2002) provide a detailed discussion of X-ray survey strategies, and Postman (2002) offers a comprehensive comparison of the X-ray, optical/NIR, and SZ approaches.

We briefly review the basic properties of cluster X-ray emission. On megaparsec scales dark matter halos collapse pulling in gas and galaxies. This gas comprises ∼85% of the luminous cluster mass, and is heated to several 10^7 K

[1] Based on observations obtained at the W.M. Keck Observatory, jointly operated by the California Institute of Technology, the University of California and the National Aeronautics and Space Administration, at the University of Hawai'i 2.2 m telescope, and at the European Southern Observatory 3.6 m on La Silla (ESO Programs 60.A-0694, 62.O-0586, 64.O-0455).

[2] European Southern Observatory, Headquarters, Karl-Schwarzschild-Strasse 2, Garching bei München D-85748, Germany, cmullis@eso.org

[3] Institute for Astronomy, University of Hawai'i, 2680 Woodlawn Drive, Honolulu, HI 96822, USA

[4] Department of Physics and Astronomy, Ohio University, Athens, OH 45701, USA

[5] Harvard-Smithsonian Center for Astrophysics, 60 Garden Street, Cambridge, MA 02138, USA

[6] Departamento de Astronomia y Astrofisica, Pontificia Universidad Catolica de Chile, Casilla 104, Santiago, 22, Chile

[7] Istituto di Radioastronomia del CNR, via Gobetti 101, Bologna, I-40129, Italy

[8] Danish Space Research Institute, Juliane Maries Vej 30, Copenhagen 0, DK-2100, Denmark

through adiabatic compression and shock heating during cluster formation. At these extreme temperatures the gas is highly ionized, optically thin ($n \sim 10^{-3}$ cm^{-3}), and primarily radiates via thermal bremsstrahlung with minor contributions from thermal line transitions (e.g., 6.7 keV Fe Kα).

The X-ray advantages of cluster selection are impressive. Clusters are very luminous (10^{43}–10^{45} erg s^{-1}) and spatially *extended* X-ray sources, which are efficiently detectable to high redshifts (e.g., RX J0848.9+4452 at $z = 1.26$, Rosati et al. 1999; Stanford et al. 2001). Since the X-ray emission is proportional to the gas density squared, clusters have relatively peaked surface-brightness profiles. This characteristic coupled with the low X-ray background nearly eliminates projection effects and underpins the high statistical quality of X-ray samples. The cosmological utility is further enhanced by the strong correlation of X-ray luminosity with cluster mass, and the fact that X-ray surveys feature well-defined selection functions. The latter is critical for reliably transforming source counts to volume-normalized diagnostics.

In this paper we present the spectroscopic redshift catalog for the 160 Square Degree *ROSAT* Cluster Survey (hereafter 160SD). The 201 galaxy clusters of the 160SD survey represent the largest, high-redshift X-ray selected sample published to date. First described by Vikhlinin et al. (1998a, hereafter V98), the 160SD clusters have been used to study the evolution of cluster X-ray luminosities and radii (Vikhlinin et al. 1998b), to present evidence for a new class of X-ray overluminous elliptical galaxies or "fossil groups" (Vikhlinin et al. 1999), to analyze the correlation of optical cluster richness with redshift and X-ray luminosity (McNamara et al. 2001), and to discover gravitational lenses (Muñoz et al. 2001; Hornstrup et al. 2003). *Chandra* observations of high-redshift 160SD clusters have been used to make an accurate determination of the evolution of the scaling relations between X-ray luminosity, temperature, and gas mass (Vikhlinin et al. 2002), and to derive cosmological constraints from the evolution of the cluster baryon mass function (Vikhlinin et al. 2003). The most recent results are reported by Mullis et al. (2003) who find significant evolution in the number density of clusters as a function of redshift based on number counts and changes in the X-ray luminosity functions.

In § 2 we review the design of the 160SD survey and describe the optical follow-up observations with an emphasis on the new spectroscopy. In § 3 we present the revised cluster catalog which features essentially complete spectroscopic redshifts. We describe the general properties of our cluster sample and compare them to the results of other X-ray surveys in § 4. We close with a brief summary in § 5. Throughout this analysis we assume an Einstein-de Sitter cosmological model with $H_0 = 50$ h$_{50}$ km s^{-1} Mpc^{-1} and $\Omega_M = 1$ ($\Omega_\Lambda = 0$), and quote X-ray fluxes and luminosities in the 0.5–2.0 keV energy band.

2. THE 160 SQUARE DEGREE ROSAT SURVEY

The study of high-redshift galaxy clusters was revolutionized by the *ROSAT* X-ray satellite (Trümper 1993) which was used to perform the first all-sky survey with an imaging X-ray telescope and to carry out a program of deep pointed observations for nearly a decade (1990–1999). These data, the *ROSAT* All-Sky Survey (RASS, Voges 1992) and the archive of pointed observations, are the basis of many X-ray selected surveys which have identified more than 1000 clusters; survey acronyms and principal references are given in Table 1. See Rosati et al. (2002) for an extensive review of the subject.

Applying different combinations of solid angle and X-ray flux sensitivity, the *ROSAT* cluster surveys provide good coverage of the X-ray luminosity-redshift parameter space. For example, BCS, CIZA, NORAS, and REFLEX adopted the wide ($\sim 10^4$ deg^2) and shallow ($f_X \gtrsim 3 \times 10^{-12}$ erg cm^{-2} s^{-1}) strategy using the RASS data to locate relatively nearby clusters ($z \lesssim 0.3$). Conversely surveys such as BMW-HRI, RDCS, SSHARC, and WARPS executed deep searches ($f_X \gtrsim 2$–6×10^{-14} erg cm^{-2} s^{-1}) with more modest solid angles ($\sim$20–200 deg^2) to identify higher redshift clusters. Our 160SD survey falls into the latter category. In the following section we review the design of the program and elaborate on the optical follow-up observations. See V98 for a complete description of the 160SD survey methodology.

2.1. *X-ray Selection of Cluster Candidates*

Clusters of galaxies are rare occurrences in the X-ray sky. Surveys such as the EMSS and NEP which have rigorously identified *all* X-ray sources within their survey regions find only $\sim$12–15% of the X-ray emitters at high Galactic latitudes are clusters (Stocke et al. 1991; Henry et al. 2001; Mullis 2001; Gioia et al. 2003). However, except for nearby, isolated elliptical galaxies, clusters are essentially the only extended X-ray sources away from the Galactic Plane. Thus with X-ray imaging data of sufficient spatial resolution and signal-to-noise, X-ray extent is an excellent means to efficiently identify galaxy clusters.

The 160SD clusters were selected based on the serendipitous detection of extended X-ray emission in 647 archival *ROSAT* PSPC observations. The search included all fields with Galactic latitude $|b| > 30°$ and hydrogen column densities $n_H < 6 \times 10^{20}$ cm^{-2} but excluded 10° radius regions around the SMC and LMC. PSPC observations targeting known clusters of galaxies, nearby galaxies, star clusters, and supernova remnants were not analyzed. A total of 160 deg^2 were surveyed at high fluxes. At lower fluxes, the sky coverage smoothly decreases due to the survey selection function (see Table 5 in V98). The area drops to 80 deg^2 at the median survey flux (1.2×10^{-13} erg cm^{-2} s^{-1}) and to 5 deg^2 at 3.7×10^{-14} erg cm^{-2} s^{-1} (which is the effective lower flux limit of the survey).

Operating on hard-band images (0.6–2.0 keV), a wavelet decomposition algorithm was used to detect X-ray sources between 2.5′ and 17.5′ from the PSPC field center. The inner radius allows for the avoidance of the original target of the pointing and the outer radius is set by the window support structure of *ROSAT* PSPC. X-ray sources significantly broader than the point-spread function (PSF), as determined through a maximum-likelihood determination, qualified for the initial list of candidate galaxy clusters.

The PSF of the *ROSAT* PSPC has a FWHM of about 25″ on-axis which grows to about 45″ at 17.5′ off axis. The radial surface-brightness profile of cluster X-ray emission is characterized by a β-model, $I(r, r_c) = I_0(1 + r^2/r_c^2)^{-3\beta+0.5}$ (Cavaliere & Fusco-

Femiano 1976). A cluster with the canonical properties (core radius r_c=250 h_{50}^{-1} kpc and slope $\beta = 2/3$) at $z = 1$ corresponds to an angular radius of $\sim 30''$ or a FWHM of $\sim 60''$ and thus is easily resolved in our survey. For a more stringent scenario consider r_c=100 h_{50}^{-1} kpc which is at the very low end of the observed distribution of core radii (e.g., Jones & Forman 1999). At $z = 1$ the intrinsic radius is $\sim 12''$. Nonetheless the convolution of the intrinsic profile and the PSF results in a significantly extended source even for this compact cluster at high redshift. The decreased detection probability for such a small cluster at larger off-axis angles is incorporated into the 160SD selection function.

It is important to recognize that though X-ray extent is the primary selection criterion for our survey, comparisons with other surveys (e.g., WARPS, Perlman et al. 2002) demonstrate that no clusters were missed as unresolved sources. Hence the results of the 160SD survey are in effect a statistically complete, X-ray flux-limited cluster sample.

2.2. *Initial Optical Follow-up Observations*

Following the X-ray selection of 223 candidate clusters, optical observations are required to verify the presence of a galaxy cluster and to estimate the distance to each system. V98 described the initial phase of these follow-up observations. A search of the NASA/IPAC Extragalactic Database (NED[9]) revealed 37 previously known clusters, 31 of which had measured redshifts in the literature. For the remaining 186 candidates, photometric CCD imaging in the R-band was obtained using the Fred Lawrence Whipple Observatory (FLWO) 1.2m, European Southern Observatory (ESO) / Danish 1.54m, and Las Campanas 1m telescopes. These were supplemented in the case of seven bright clusters using the DSS-II plates which can be used to identify clusters to $z \lesssim 0.45$. The CCD imaging was sufficiently deep to reveal clusters to $z = 0.7 - 0.9$. Figure 1 illustrates the relative ease of establishing the presence of distant clusters even with short exposures through a modest telescope. An overdensity of galaxies visible in this 5 minute R-band image from the FLWO 1.2m is perfectly aligned with the X-ray emission from an 80 ks *Chandra* observation. Our subsequent Keck-II longslit spectra (Figure 2) taken along the major axis of the X-rays and galaxy distribution confirm the presence of a cluster at $z = 0.700$. If a concentration of galaxies is not present in the CCD imaging it was classified as a false detection though it could presumably be a very distant cluster (e.g., RX J0848.9+4452 which is 160SD cluster #61 at $z = 1.26$).

In total 203 clusters were confirmed by V98 (see Table 2). Of the remaining 20 sources, 19 are probable false detections resulting from the blends of unresolved X-ray point sources. It was not possible to confirm RX J1415.6+1906 (#157) because it is obscured by the glare of Arcturus. The exceptional quality of the 160SD X-ray selection is reinforced by this high success rate (91%).

The second phase of the optical follow-up concerns spectroscopic measurements principally used to measure distances to the clusters. Of course the determination of concordant redshifts from amongst the likely cluster members further justifies the cluster classification, but this is somewhat ancillary given the presence of extended X-ray emission spatially coincident with a galaxy density enhancement. As previously noted, spectroscopic redshifts for 31 of the clusters were available from the literature. V98 obtained spectroscopic redshifts for 45 additional clusters using the Multiple Mirror Telescope 6×1.8m, ESO 3.6m, and ESO/Danish 1.54m telescopes, and presented photometric redshifts for 124 of the remaining 127 clusters based on the magnitude of the brightest cluster galaxy (BCG). Reliable photometric estimates were not possible for three candidates RX J0910.6+4248 (#69), RX J1237.4+11141 (#122), and RX J1438.9+6423 (#164) because the selection of the BCG in each case was unclear due to the large angular extent of the candidate. Note the object identification numbers in parentheses are the same as the ones used in V98. The distance estimates of V98 are summarized in the second column of Table 3.

The membership of the 160SD cluster sample has proven to be remarkably stable since first presented by V98. Based on the results of extensive spectroscopic follow-up (described in § 2.3), the revised sample consists of 201 confirmed clusters, 21 false detections, and one source obscured by Arcturus (see Table 2). These classifications have changed very little; one probable false detection has been identified as a cluster and three cluster candidates have been reclassified as probable falses. RX J0848.9+4452 (#61) was originally classified as a probable false detection because no galaxy overdensity was visible in our optical image of this field. However, it was forewarned that such an object could be a very distant ($z \gtrsim 0.9$) cluster. In fact Rosati et al. (1999) have proven that this X-ray source is a cluster at $z = 1.26$ making it the most distant system found in any of the X-ray surveys thus far. RX J0857.7+2747 (#65), RX J1429.6+4234 (#163), and RX J2004.8-5603 (#197) were initially cluster candidates but we now interpret them to be likely false detections because our spectroscopic survey of these fields failed to find any coherent structure in redshift space.

2.3. *New Spectroscopic Redshifts*

Since the initial follow-up observations we have gone on to measure spectroscopic redshifts for 110 additional clusters from our 160SD survey using the Keck-II 10m and the University of Hawai'i (UH) 2.2m telescopes at the Mauna Kea Observatories, and the ESO 3.6m telescope at La Silla Observatory. Combining these new redshifts with 76 measurements reported by V98 and 14 redshifts from the literature and private communications results in essentially complete (200 of 201 clusters) spectroscopic coverage for our entire sample. Refer to Table 3 for a summary of the redshift determinations. The new cluster catalog will be presented in § 3. Here we give a technical description of the new observations.

We chose the targets for the low-dispersion spectroscopic observations using our previously described CCD images. This was usually a straightforward task since in most cases unambiguous cluster members were spatially coincident with the extended X-ray emission. Longslit spectra were obtained with the Keck-II 10m and the UH 2.2m resulting

[9] http://nedwww.ipac.caltech.edu/

in usually 2–3 concordant galaxy redshifts per cluster, and always including the BCG. Longslit and multi-object spectra were taken with the ESO 3.6m, the latter producing 10–15 galaxy redshifts per cluster.

We measured redshifts for the most distant clusters ($z \gtrsim 0.5$) using the Keck-II 10m telescope with the Low Resolution Imaging Spectrometer (LRIS, Oke et al. 1995) during four nights of observations (1999 July 07–08 and 2000 January 26–27). Examples are shown in Figures 2 and 4. The 300 lines mm^{-1} grating (5000Å blaze) combined with the GG495 long-pass order-blocking filter yielded an effective wavelength coverage of approximately 5000Å–9000Å and a dispersion of 2.45Å pixel^{-1}. With the Tektronix 2048×2048 CCD detector the spatial scale is 0.215″ pixel^{-1}. We used a slit of 1.5″ in width, which gives a reduced spectral resolution of ∼16Å FWHM ($R \sim 440$). Exposure times were typically 1200s–2400 s and the seeing was 0.7″– 1.1″.

Moderately distant clusters were observed using the UH 2.2m with the Wide Field Grism Spectrograph (WFGS) during ten nights of spectroscopy (1998 May – 2000 February). The instrument setup consisted of the Tektronix 2048×2048 CCD at the f/10 focus with the 420 lines mm^{-1} red grism and a 1.8″ slit, providing a wavelength coverage of approximately 3800Å–9000Å. The spectral dispersion is 3.6Å pixel^{-1}, the spectral resolution is ∼19Å FWHM ($R \sim 340$), and the spatial scale is 0.35″ pixel^{-1}. The typical seeing was 0.8″–1.5″ and integration times ranged between 600s and 3600 s.

We observed the southern clusters not visible from Mauna Kea using the ESO 3.6m with the ESO Faint Object Spectrograph and Camera (EFOSC2), in both the longslit and the multi-object spectroscopy modes. Data were taken over 6 nights (1998 March 28, 1999 February 15–16, and 1999 November 06–08) during which time the seeing varied over the range 0.6″–1.8″. The 300 lines mm^{-1} grating (#6, 5000Å blaze) with a 1.5″ slit provides a wavelength coverage of about 3900Å–8000Å with a spectral resolution of ∼20Å ($R \sim 300$). The spectral dispersion is 4Å pixel^{-1} and the spatial scale is 0.31″ pixel^{-1} using the Loral 2048×2048 CCD binned 2×2 at readout. Exposure times were usually between 900s and 1800s.

In total we observed over 400 individual galaxies to derive the 110 new cluster redshifts reported in this paper. The only cluster for which we lack a redshift is RX J1237.4+1141 (#122). The unusually large extent of this source would require an extensive redshift survey to yield a reliable distance measurement. We analyzed our data following standard procedures using IRAF[10] reduction packages and IDL[11] routines. Two-dimensional spectra were de-biased and flat-fielded. One-dimensional spectra, with the sky background subtracted, were extracted and wavelength calibrated. Finally the instrumental response was removed using observations of the spectrophotometric standard stars of Oke & Gunn (1983) and Massey et al. (1988). Redshifts were measured based on the offsets of absorption features commonly observed in early-type galaxies including the Ca II H and K doublet (3933.68Å, 3968.49Å), the 4000Å break, the CH G band (∼4300Å), Mg Ib (∼5175Å), and Na Id (5889.97Å).

Brief descriptions of a few individual clusters demonstrate the reliability of our X-ray source characterization and the rigor of our optical follow-up program. Though relatively simple X-ray/optical configurations such as that shown in Figure 1 are the most commonly observed, there are more challenging scenarios. Take for instance the 160SD source RX J0921.2+4528 (#70). We were surprised when our spectrum of the apparent BCG revealed a broad-line QSO at $z = 1.66$. Since active galactic nuclei (AGN) are usually X-ray luminous we could have stopped here and classified RX J0921.2+4528 as an AGN. However our analysis of the X-ray data shows this source is significantly (6σ) broader than the *ROSAT* PSPC PSF thus motivating us to pursue this further. With subsequent spectroscopy we found five concordant redshifts at $z = 0.315$ confirming the cluster identification. More interestingly, a second QSO at $z = 1.66$ was found separated 6.93″ from the first. Muñoz et al. (2001) further describe this wide-separation gravitational lens candidate. Our Monte-Carlo simulations show that a 90% upper limit on the flux of a point source at the QSO position is about 35% of the total cluster flux.

Another complex source to disentangle is RX J1524.6+0957 (#170). With a cursory inspection of the I-band image shown in Figure 3 one might conclude the obvious low-redshift group is the optical counterpart of the X-ray source. This interpretation was reported by the BSHARC survey who quoted a redshift of $z = 0.078$ (Romer et al. 2000). However, closer scrutiny of the fainter objects suggests a concentration of galaxies at the X-ray position. Our Keck-II spectroscopy for these faint galaxies establishes a distant cluster at $z = 0.516$ (Figure 4). Were the nearby group the principal source of the X-rays, it would have to be exceedingly compact. The measured core radius of 26″ corresponds to 52 h_{50}^{-1} kpc at $z = 0.078$ or 190 h_{50}^{-1} kpc at $z = 0.516$. The former is unrealistic whereas the latter is quite typical. Finally, we measure an ∼5 keV temperature for the intracluster medium, via a spectral fit to the *Chandra* data, which strongly rejects the group-dominant scenario. Thus we conclude the primary identification for RX J1524.6+0957 is a distant cluster at $z = 0.516$.

We close this section with an assessment of the photometric redshift estimates of V98 versus the spectroscopic measurements reported here. Looking at the relevant data plotted in Figure 5 we see that in general the photometric redshifts were quite reliable. In retrospect the 90% confidence interval of $\Delta z = {}^{+0.04}_{-0.07}$ for the 117 CCD-based estimates was somewhat underestimated by V98, since only 70% of the spectroscopic redshifts actually fall within this error range. Ignoring the six principal outlyers labeled in Figure 5, the true 90% confidence interval is about $\Delta z = \pm 0.1$.

3. REVISED CLUSTER CATALOG WITH SPECTROSCOPIC REDSHIFTS AND X-RAY LUMINOSITIES

We present the revised cluster catalog for the 160SD survey in Table 4. The most significant feature is the nearly

[10] IRAF is distributed by the National Optical Astronomy Observatories, which are operated by the Association of Universities for Research in Astronomy, Inc., under cooperative agreement with the National Science Foundation. http://iraf.noao.edu

[11] http://www.rsinc.com, http://idlastro.gsfc.nasa.gov/homepage.html

complete spectroscopic coverage. We report spectroscopic redshifts for 200 of the 201 (99.5%) clusters in our sample. With knowledge of the cluster distances we can compute accurate X-ray luminosities. Hence the fundamental parameters are now available to pursue detailed investigations with this statistically complete, X-ray flux-limited sample.

In Table 4 we provide detailed information for each of the 201 clusters discovered in the 160SD survey. For completeness we also list the 22 other objects meeting our original selection criteria of significant X-ray extent. Twenty-one of these, flagged with "F" in columns (10), (11), and (13), are likely false detections due to blends of unresolved X-ray point sources. The other source is only 4.4′ away from the zero magnitude star Arcturus and hence nearly impossible to confirm as a cluster.

The object name and object number are given in columns (1) and (2). Note the latter is the same identification used by V98. The right ascension and declination (J2000) for the centroid of the X-ray emission are listed in columns (3) and (4). Column (5) gives the positional uncertainty in terms of the radius for the 90% confidence X-ray position error circle. Columns (6) and (7) give the angular core radius and its uncertainty based on a β-model fit with $\beta = 2/3$. The total, unabsorbed X-ray flux in the 0.5–2.0 keV energy band in the observer's restframe and its uncertainty are listed in columns (8) and (9).

Cluster X-ray luminosity in the 0.5–2.0 keV energy band is reported in column (10). Luminosity in the object's rest frame is defined by

$$L_{\rm X} \;=\; 4\pi d_{\rm L}^2 \; f_{\rm X} \; k_{\,0.5-2.0} \qquad (1)$$

where $f_{\rm X}$ is the total X-ray flux, $d_{\rm L}$ is the luminosity distance (e.g., Weinberg 1972), and $k_{\,0.5-2.0}$ is the K-correction in the 0.5 – 2.0 keV band. The latter transforms the *ROSAT* rest-frame luminosity into the object's rest-frame luminosity. The K-correction here is given by

$$k_{\,0.5-2.0} \;=\; \frac{\int_{0.5}^{2.0} f_{\rm E} d{\rm E}}{\int_{0.5(1+z)}^{2.0(1+z)} f_{\rm E} d{\rm E}} \qquad (2)$$

where $f_{\rm E}$ is the differential flux (flux per unit energy) as a function of energy and the integration limits are energy band edges in keV. The K-corrections for clusters, shown in Figure 6, were computed assuming a Raymond-Smith plasma spectrum (Raymond & Smith 1977) with a metallicity of 0.3 solar and a gas temperature for the intracluster medium (ICM) consistent with the $L_{\rm X}$–kT relation of White, Jones, & Forman (1997),

$$kT = 2.76\,{\rm keV}\; L_{\rm X,bol,44}^{0.33}, \qquad (3)$$

where $L_{\rm X,bol,44}$ is the bolometric X-ray luminosity in units of 10^{44} erg s^{-1} with $H_0 = 50$ h$_{50}$ km s^{-1} Mpc^{-1}

Heliocentric spectroscopic redshifts which entirely supersede the photometric estimates of V98 are given in column (11). We measured redshifts for 155 clusters while 45 come from the literature and private communications as referenced in column (12). In a few cases the precision of literature-based redshifts reported by V98 have been updated to reflect more robust measurements that are now available.

The final column (13) lists notes on individual clusters. In particular we indicate where our 160SD clusters are also members of other X-ray selected samples. Coincidences were found with the BCS+eBCS (Ebeling et al. 1998, 2000), BMW-HRI (L. Guzzo, priv. comm.), BSHARC (Romer et al. 2000), EMSS (Gioia & Luppino 1994), NORAS (Böhringer et al. 2000), RBS (Schwope et al. 2000), RDCS (P. Rosati, priv. comm.), REFLEX-I/II (H. Böhringer, priv. comm.), RIXOS (Mason et al. 2000), SSHARC (Burke et al. 2003), and WARPS-I/II (Perlman et al. 2002; L. Jones, priv. comm.). No matches were found in the MACS (H. Ebeling, priv. comm.), the NEP (Mullis 2001; Gioia et al. 2003), RASS1BS (De Grandi et al. 1999) or the SGP (Cruddace et al. 2002, 2003) samples.

We also mark in column (13) the four X-ray overluminous elliptical galaxies (OLEGs) described by Vikhlinin et al. (1999) which are potential "fossil groups" similar to those reported by others (e.g., Jones, Ponman, & Forbes 2000, Romer et al. 2000, Mullis 2001). Finally, we note nine instances where the cluster redshift is within $\Delta z = 0.015$ of the original target of the *ROSAT* PSPC pointed observations (flagged with "$z_{\rm PSPC}$").

4. DISCUSSION

We describe here the general properties of our cluster sample and compare them to the results of other X-ray surveys. In Figure 7 we plot the luminosity-redshift distribution for 160SD clusters. The median redshift is $z_{\rm median} = 0.25$ and the median X-ray luminosity is $L_{\rm X,median} = 4.2 \times 10^{43}$ h$_{50}^{-2}$ erg s^{-1}. Note that the 160SD sample is the largest high-redshift sample of X-ray-selected clusters published to date. For example there are 73 clusters at $z > 0.3$ and 22 clusters at $z > 0.5$.

As remarked by Vikhlinin et al. (2003) the *ROSAT* fluxes (and by inference luminosities) used in our survey construction show very good agreement with those measured in deep *Chandra* observations. For the six 160SD clusters observed by both X-ray telescopes (as of early 2003), the fluxes differ by $\leq$13%, with no systematic offset, and always within the statistical uncertainties. Comparisons of fluxes independently measured from *ROSAT* observations demonstrate consistent results. For example, using appropriate core radii and redshifts, Romer et al. (2000) report no systematic offsets between their measurements and ours for 11 clusters which are common to the BSHARC and 160SD surveys. Examining 16 clusters detected in the 20 *ROSAT* fields surveyed by both WARPS-I and 160SD, Perlman et al. (2002) find a mean flux ratio of $f_{\rm 160SD}/f_{\rm WARPS} = 0.98 \pm 0.26$. We compared our fluxes to those of the SSHARC survey (Burke et al. 2003) and find for the nine shared clusters the mean flux ratio is $f_{\rm 160SD}/f_{\rm SSHARC} = 0.78 \pm 0.22$. This tendency for the SSHARC fluxes to be somewhat larger than those of the 160SD and other surveys is also noted by Burke et al. (2003).

The statistics concerning the membership of the 160SD clusters in other samples are summarized in Table 5. Six independent cluster surveys, including the 160SD, have been extracted from the same parent dataset, the *ROSAT* archive of pointed PSPC observations. Thus a significant amount of shared objects is anticipated and is confirmed. Given the large solid angle and deep flux limit of our survey, the 201 clusters of 160SD comprise the largest sample

derived from the PSPC archive and encompass approximately 30%–60% of the clusters from similar surveys. By number the largest overlap is 46 clusters shared with the RDCS, whereas by percentage the largest coincidence is the 58% of RIXOS clusters. Not surprisingly there are much fewer matches between the 160SD catalog and the surveys based on the RASS. The 160 deg^2 sky coverage of our survey is a very small fraction of the near all-sky coverage of the RASS. Furthermore, these RASS-based surveys are largely dominated by nearby ($z \lesssim 0.3$) bright clusters, which were often the target of PSPC observations and thus excluded by design from the 160SD sample. Finally, there are only minor duplications between the *ROSAT* PSPC and the *ROSAT* HRI or *Einstein* IPC pointings, hence the overlaps with the EMSS and BMW-HRI samples are small.

Since the 160SD cluster sample was the first of the *ROSAT* surveys to be published (V98), subsequent groups have had the opportunity to make detailed comparisons to our sample (e.g., BSHARC: Romer et al. 2000; SSHARC: Burke et al. 2003; WARPS-I: Perlman et al. 2002). In each case the authors have made a field-by-field evaluation of their X-ray source detections and cluster identifications versus ours for the *ROSAT* pointings common to both surveys. We highlight and further develop the key results using the revised 160SD catalog.

There are 201 *ROSAT* PSPC fields processed by both the BSHARC and 160SD surveys (Romer et al. 2000, see their § 7.5). Note the BSHARC survey adopted a wide and shallow strategy covering approximately 178 deg^2 above a flux limit of $\sim 3 \times 10^{-13}$ erg s^{-1}. In the shared area there are twenty-one 160SD clusters which are sufficiently bright as to appear in the BSHARC survey. Thirteen of these X-rays sources are recovered in the BSHARC sample, whereas eight are missing. Six clusters (#9, #42, #107, #182, #195, and #207) were not included because of a failure to meet a filling factor criterion, and two (#110 and #201) were missed because they were not detected as extended (Romer et al. 2000; K. Romer, priv. comm.). The BSHARC filling factor diagnostic was used to reject blends or "percolation runaways"; see Perlman et al. (2002) for a discussion on the impact of this filter on survey completeness. For the thirteen sources successfully detected by the BSHARC survey, we note only two deviations in the optical identifications. First, RX J0947.7+0741 (#75) is identified as a QSO at $z = 0.63$, but we have measured concordant galaxy redshifts at $z = 0.625$ thus suggesting that the extended X-ray emission is the result of the ICM. The QSO was in fact identified as a separate point source by our X-ray analysis software. Second as previously discussed in § 2.3, RX J1524.6+0957 (#170) is listed as a group at $z = 0.078$ whereas we conclude that a $z = 0.516$ cluster is the dominant source. Romer et al. (2000) did not identify any additional clusters within 160SD survey boundaries which are not already part of the 160SD catalog.

Recently Burke et al. (2003, see latter portions of their § 3.1 and § 4) described the results of the SSHARC project and examined the areas of the sky jointly surveyed by both the SSHARC and 160SD. Note that both surveys probe to similar lower flux limits ($\sim 4 \times 10^{-14}$ erg cm^{-2} s^{-1}) but the SSHARC was limited to a relatively small solid angle of 17.7 deg^2. There are sixteen 160SD clusters in the overlap region. Nine of these are identified as clusters in the SSHARC sample whereas seven are missing. One 160SD cluster (#215), which is also a part of the RDCS sample, was not detected in the SSHARC survey. The remaining six (#39, #43, #75, #83, #124, and #214) were flagged as extended X-ray sources by Burke et al. (2003); however they concluded that their optical follow-up does not suggest the existence of a cluster in any of these cases. Nonetheless, we have measured multiple concordant redshifts for each of these six clusters. Also note clusters #83 and #124 are confirmed members of the WARPS-II and RDCS samples, respectively. Burke et al. (2003) point out one SSHARC cluster (RX J0505.3-2849, $z = 0.509$) which should formally meet our selection criteria but was not included in our catalog because it was detected as two separate sources. We manually inspected the processed *ROSAT* fields during survey construction and suspected this double source was an incorrect result of the X-ray detection algorithm. However, no other similar cases were found in the entire survey, and we opted not to modify the detection software for the sake of this single relatively X-ray faint cluster.

The first phase of the WARPS survey (Perlman et al. 2002, and references therein) is similar in sky coverage to the SSHARC. WARPS-I covered 16.2 deg^2 down to a flux limit of 6.5×10^{-14} erg s^{-1} in total flux. The ongoing second phase, WARPS-II, extends the survey area to about 73 deg^2 (H. Ebeling, priv. comm.). Perlman et al. (2002) scrutinized the 20 *ROSAT* PSPC fields included in both the 160SD and WARPS-I surveys. They found that the 16 cluster identifications in the overlap region are in complete agreement. Furthermore, we note excellent accord in the cluster redshifts except in one case. For RX J0210.4-3929 (#25) we measured a redshift for the BCG of $z = 0.165$ and obtained a low signal-to-noise spectrum of a second galaxy that is consistent with the BCG redshift. In the WARPS-I catalog (Perlman et al. 2002) the redshift is quoted as $z = 0.273$ but is noted to be uncertain. In light of our new evidence the WARPS team re-examined their low-quality spectra for this cluster and find their data are consistent with the 160SD redshift (E. Perlman, priv. comm.).

Finally, we emphasize a very important conclusion that can be drawn from the careful work of the WARPS program. Their survey is unique amongst the complement of cluster searches based upon the *ROSAT* PSPC archive of pointed observations in that they pursued optical identifications for extended X-ray sources as well as for *non*-extended sources. The others, including the 160SD survey, only examined X-ray emitters which were significantly extended. The fact that the WARPS team found no clusters missed by the 160SD, and in particular, no cluster was missed because it was not resolved as extended, underscores the completeness of our survey strategy.

5. SUMMARY

We present the revised catalog of 201 galaxy clusters for the 160SD survey featuring spectroscopic redshifts for 99.5% of the members. This sample includes 30%–60% of the clusters from similar *ROSAT* cluster surveys, and is currently the largest high-redshift sample of X-ray se-

lect clusters in the public domain. We review the X-ray criteria used to locate these galaxy systems, describe the optical imaging and spectroscopy used to classify them, and compare our results with similar studies.

It is a pleasure to thank Piero Rosati, Hans Böhringer, Harald Ebeling, Kathy Romer, Eric Perlman, Stefano Ettori and Axel Schwope for fruitful discussions. We are grateful to Harald Ebeling and the WARPS team, Piero Rosati and the RDCS team, and John Huchra for sharing cluster redshifts prior to publication (respectively 3, 1, and 2 entries referenced in Table 4). Kathy Romer and the BSHARC team kindly shared galaxy redshifts for the foreground group associated with RX J1524.6+0957. We thank Piero Rosati and the RDCS team for providing the unpublished RDCS sample, and Laurence Jones and the WARPS team for providing access to the unpublished WARPS-II sample to permit cross-correlations with the 160SD clusters. Similarly we appreciate Luigi Guzzo and the BMW-HRI team for sharing the target list for their on-going survey for comparison with the 160SD. Hans Böhringer kindly provided the cross correlation of the unpublished REFLEX-I/II samples and the 160SD clusters. The referee is thanked for providing comments that helped clarify the presentation of this work. The support of the time allocation committees at UH and ESO, and the expertise of the dedicated personnel at the Mauna Kea and La Silla observatories are gratefully acknowledged. The authors recognize the religious and cultural significance of the summit of Mauna Kea to the indigenous people of Hawai'i. We deeply appreciate the opportunity to pursue scientific research from this special place.

C.R.M. acknowledges partial financial support from NASA grant NGT5-50175, the ESO Office for Science, and the ARCS Foundation. The contributions of B.R.M., A.V., W.R.F., and C.J.F. were possible thanks in part to NASA grant NAG5-9217 and contract NAS8-39073. HQ was partially supported by FONDAP Centro de Astrofisica. This research has made use of the NASA/IPAC Extragalactic Database (NED) which is operated by the Jet Propulsion Laboratory, California Institute of Technology, under contract with the National Aeronautics and Space Administration.

REFERENCES

Abell, G. O., Corwin, H. G., & Olowin, R. P. 1989, ApJS, 70, 1
Allen, S. W., Ettori, S., & Fabian, A. C. 2001, MNRAS, 324, 877
Böhringer, H., Schuecker, P., Guzzo, L., Collins, C. A., Voges, W., Schindler, S., Neumann, D. M., Cruddace, R. G., De Grandi, S., Chincarini, G., Edge, A. C., MacGillivray, H. T., & Shaver, P. 2001, A&A, 369, 826
Böhringer, H., Voges, W., Huchra, J. P., McLean, B., Giacconi, R., Rosati, P., Burg, R., Mader, J., Schuecker, P., Simic, D., Komossa, S., Reiprich, T. H., Retzlaff, J., & Trümper, J. 2000, ApJS, 129, 435
Bond, J. R., Kofman, L., & Pogosyan, D. 1996, Nature, 380, 603
Borgani, S. & Guzzo, L. 2001, Nature, 409, 39
Borgani, S., Rosati, P., Tozzi, P., Stanford, S. A., Eisenhardt, P. R., Lidman, C., Holden, B., Della Ceca, R., Norman, C., & Squires, G. 2001, ApJ, 561, 13
Boyle, B. J., Wilkes, B. J., & Elvis, M. 1997, MNRAS, 285, 511
Burke, D. J., Collins, C. A., Sharples, R. M., Romer, A. K., & Nichol, R. C. 2003, MNRAS, accepted
Carlstrom, J. E., Holder, G. P., & Reese, E. D. 2002, ARA&A, 40, 643
Castander, F. J., Bower, R. G., Ellis, R. S., Aragon-Salamanca, A., Mason, K. O., Hasinger, G., McMahon, R. G., Carrera, F. J., Mittaz, J. P. D., Perez-Fournon, I., & Lehto, H. J. 1995, Nature, 377, 39
Cavaliere, A. & Fusco-Femiano, R. 1976, A&A, 49, 137
Clowe, D. & Schneider, P. 2002, A&A, 395, 385
Couch, W. J., Ellis, R. S., MacLaren, I., & Malin, D. F. 1991, MNRAS, 249, 606
Cruddace, R., Voges, W., Böhringer, H., Collins, C. A., Romer, A. K., MacGillivray, H., Yentis, D., Schuecker, P., Ebeling, H., & De Grandi, S. 2002, ApJS, 140, 239
—. 2003, ApJS, 144, 299
Czoske, O., Moore, B., Kneib, J.-P., & Soucail, G. 2002, A&A, 386, 31
De Grandi, S., Böhringer, H., Guzzo, L., Molendi, S., Chincarini, G., Collins, C., Cruddace, R., Neumann, D., Schindler, S., Schuecker, P., & Voges, W. 1999, ApJ, 514, 148
Donahue, M., Mack, J., Scharf, C., Lee, P., Postman, M., Rosati, P., Dickinson, M., Voit, G. M., & Stocke, J. T. 2001, ApJ, 552, L93
Donahue, M., Scharf, C. A., Mack, J., Lee, Y. P., Postman, M., Rosati, P., Dickinson, M., Voit, G. M., & Stocke, J. T. 2002, ApJ, 569, 689
Ebeling, H., Edge, A. C., Allen, S. W., Crawford, C. S., Fabian, A. C., & Huchra, J. P. 2000, MNRAS, 318, 333
Ebeling, H., Edge, A. C., Bohringer, H., Allen, S. W., Crawford, C. S., Fabian, A. C., Voges, W., & Huchra, J. P. 1998, MNRAS, 301, 881
Ebeling, H., Edge, A. C., & Henry, J. P. 2001, ApJ, 553, 668
Ebeling, H., Mullis, C. R., & Tully, R. B. 2002, ApJ, 580, 774
Gioia, I. M., Henry, J. P., Maccacaro, T., Morris, S. L., Stocke, J. T., & Wolter, A. 1990, ApJ, 356, L35
Gioia, I. M., Henry, J. P., Mullis, C. R., Ebeling, H., & Wolter, A. 1999, AJ, 117, 2608
Gioia, I. M., Henry, J. P., Mullis, C. R., Voges, W., Briel, U. G., Böhringer, H., & Huchra, J. P. 2003, ApJS, submitted
Gioia, I. M. & Luppino, G. A. 1994, ApJS, 94, 583
Griffiths, R. E., Tuohy, I. R., Brissenden, R. J. V., & Ward, M. J. 1992, MNRAS, 255, 545
Henry, J. P. 2000, ApJ, 534, 565
Henry, J. P., Gioia, I. M., Maccacaro, T., Morris, S. L., Stocke, J. T., & Wolter, A. 1992, ApJ, 386, 408
Henry, J. P., Gioia, I. M., Mullis, C. R., Voges, W., Briel, U. G., Böhringer, H., & Huchra, J. P. 2001, ApJ, 553, L109
Hornstrup, A., McNamara, B. R., Vikhlinin, A., Greve, T. R., Forman, W. R., & Jones, C. 2003, ApJ, submitted
Huchra, J. P., Geller, M. J., Henry, J. P., & Postman, M. 1990, ApJ, 365, 66
Huchra, J. P., Vogeley, M. S., & Geller, M. J. 1999, ApJS, 121, 287
Jenkins, A., Frenk, C. S., Pearce, F. R., Thomas, P. A., Colberg, J. M., White, S. D. M., Couchman, H. M. P., Peacock, J. A., Efstathiou, G., & Nelson, A. H. 1998, ApJ, 499, 20
Jones, C. & Forman, W. 1999, ApJ, 511, 65
Jones, L. R., Ponman, T. J., & Forbes, D. A. 2000, MNRAS, 312, 139
Kopylov, A. I., Fetisova, T. S., & Shvartsman, V. F. 1984, Astronomicheskij Tsirkulyar, 1344, 1
Kurtz, M. J., Huchra, J. P., Beers, T. C., Geller, M. J., Gioia, I. M., Maccacaro, T., Schild, R. E., & Stauffer, J. R. 1985, AJ, 90, 1665
Loveday, J., Peterson, B. A., Maddox, S. J., & Efstathiou, G. 1996, ApJS, 107, 201
Mahdavi, A., Böhringer, H., Geller, M. J., & Ramella, M. 2000, ApJ, 534, 114
Markevitch, M., Gonzalez, A. H., David, L., Vikhlinin, A., Murray, S., Forman, W., Jones, C., & Tucker, W. 2002, ApJ, 567, L27
Mason, K. O., Carrera, F. J., Hasinger, G., Andernach, H., Aragon-Salamanca, A., Barcons, X., Bower, R., Brandt, W. N., Branduardi-Raymont, G., Burgos-Martín, J., Cabrera-Guerra, F., Carballo, R., Castander, F., Ellis, R. S., González-Serrano, J. I., Martínez-González, E., Martín-Mirones, J. M., McMahon, R. G., Mittaz, J. P. D., Nicholson, K. L., Page, M. J., Pérez-Fournon, I., Puchnarewicz, E. M., Romero-Colmenero, E., Schwope, A. D., Vila, B., Watson, M. G., & Wonnacott, D. 2000, MNRAS, 311, 456
Massey, P., Strobel, K., Barnes, J. V., & Anderson, E. 1988, ApJ, 328, 315
McHardy, I. M., Jones, L. R., Merrifield, M. R., Mason, K. O., Newsam, A. M., Abraham, R. G., Dalton, G. B., Carrera, F., Smith, P. J., Rowan-Robinson, M., & Abraham, R. G. 1998, MNRAS, 295, 641
McNamara, B. R., Vikhlinin, A., Hornstrup, A., Quintana, H., Whitman, K., Forman, W., & Jones, C. 2001, ApJ, 558, 590

Moretti, A., Guzzo, L., Campana, S., Covino, S., Lazzati, D., Longhetti, M., Molinari, E., Panzera, M. R., Tagliaferri, G., & dell'Antonio, I. 2001, in ASP Conf. Ser. 234: X-ray Astronomy 2000, 393
Muñoz, J. A., Falco, E. E., Kochanek, C. S., Lehár, J., McLeod, B. A., McNamara, B. R., Vikhlinin, A. A., Impey, C. D., Rix, H. ., Keeton, C. R., Peng, C. Y., & Mullis, C. R. 2001, ApJ, 546, 769
Mulchaey, J. S. 2000, ARA&A, 38, 289
Mullis, C. R. 2001, Ph.D. Thesis, Univ. of Hawaii
Mullis, C. R., Henry, J. P., Gioia, I. M., Böhringer, H., Briel, U. G., Voges, W., & Huchra, J. P. 2001, ApJ, 553, L115
Mullis, C. R., Vikhlinin, A., Henry, J. P., McNamara, B. R., Quintana, H., Gioia, I. M., Hornstrup, A., Way, M., Forman, W., & Jones, C. 2003, in preparation
Nesci, R. & Altamore, A. 1990, A&A, 234, 60
Oegerle, W. R., Hill, J. M., & Fitchett, M. J. 1995, AJ, 110, 32+
Oke, J. B., Cohen, J. G., Carr, M., Cromer, J., Dingizian, A., Harris, F. H., Labrecque, S., Lucinio, R., Schaal, W., Epps, H., & Miller, J. 1995, PASP, 107, 375
Oke, J. B. & Gunn, J. E. 1983, ApJ, 266, 713
Panzera, M. R., Campana, S., Covino, S., Lazzati, D., Mignani, R. P., Moretti, A., & Tagliaferri, G. 2003, A&A, 399, 351
Peacock, J. A. 1999, Cosmological Physics (Cambridge, UK: Cambridge University Press)
Peebles, P. J. E. 1993, Principles of Physical Cosmology (Princeton, NJ: Princeton University Press)
Perlman, E. S., Horner, D. J., Jones, L. R., Scharf, C. A., Ebeling, H., Wegner, G., & Malkan, M. 2002, ApJS, 140, 265
Ponman, T. J., Allan, D. J., Jones, L. R., Merrifield, M., McHardy, I. M., Lehto, H. J., & Luppino, G. A. 1994, Nature, 369, 462
Postman, M. 2002, in ASP Conf. Ser. TBD: Tracing Cosmic Evolution with Galaxy Clusters, 1
Quintana, H. & Ramirez, A. 1995, ApJS, 96, 343
Raymond, J. C. & Smith, B. W. 1977, ApJS, 35, 419
Romer, A. K., Nichol, R. C., Holden, B. P., Ulmer, M. P., Pildis, R. A., Merrelli, A. J., Adami, C., Burke, D. J., Collins, C. A., Metevier, A. J., Kron, R. G., & Commons, K. 2000, ApJS, 126, 209
Rosati, P., Borgani, S., & Norman, C. 2002, ARA&A, 40, 539
Rosati, P., della Ceca, R., Burg, R., Norman, C., & Giacconi, R. 1995, ApJ, 445, L11
Rosati, P., della Ceca, R., Norman, C., & Giacconi, R. 1998, ApJ, 492, L21
Rosati, P., Stanford, S. A., Eisenhardt, P. R., Elston, R., Spinrad, H., Stern, D., & Dey, A. 1999, AJ, 118, 76
Rose, J. A., Gaba, A. E., Christiansen, W. A., Davis, D. S., Caldwell, N., Hunstead, R. W., & Johnston-Hollitt, M. 2002, AJ, 123, 1216
Sarazin, C. L. 1988, X-ray emission from clusters of galaxies (Cambridge Astrophysics Series, Cambridge: Cambridge University Press)
Scharf, C. A., Jones, L. R., Ebeling, H., Perlman, E., Malkan, M., & Wegner, G. 1997, ApJ, 477, 79
Schmidt, M., Hasinger, G., Gunn, J., Schneider, D., Burg, R., Giacconi, R., Lehmann, I., MacKenty, J., Trumper, J., & Zamorani, G. 1998, A&A, 329, 495
Schneider, D. P., Gunn, J. E., & Hoessel, J. G. 1983, ApJ, 264, 337
Schwope, A., Hasinger, G., Lehmann, I., Schwarz, R., Brunner, H., Neizvestny, S., Ugryumov, A., Balega, Y., Trümper, J., & Voges, W. 2000, AN, 321, 1
Silk, J. & White, S. D. M. 1978, ApJ, 226, L103
Smail, I., Ellis, R. S., Dressler, A., Couch, W. J., Oemler, A. J., Sharples, R. M., & Butcher, H. 1997, ApJ, 479, 70
Stanford, S. A., Holden, B., Rosati, P., Tozzi, P., Borgani, S., Eisenhardt, P. R., & Spinrad, H. 2001, ApJ, 552, 504
Stocke, J. T., Morris, S. L., Gioia, I. M., Maccacaro, T., Schild, R., Wolter, A., Fleming, T. A., & Henry, J. P. 1991, ApJS, 76, 813
Struble, M. F. & Rood, H. J. 1999, ApJS, 125, 35
Sunyaev, R. A. & Zeldovich, Y. B. 1972, Com.Ap, 4, 173
Trümper, J. 1993, Science, 260, 1769
Ulrich, M.-H. 1976, ApJ, 206, 364
Vikhlinin, A., Markevitch, M., & Murray, S. S. 2001, ApJ, 551, 160
Vikhlinin, A., McNamara, B. R., Forman, W., Jones, C., Quintana, H., & Hornstrup, A. 1998a, ApJ, 502, 558
—. 1998b, ApJ, 498, L21
Vikhlinin, A., McNamara, B. R., Hornstrup, A., Quintana, H., Forman, W., Jones, C., & Way, M. 1999, ApJ, 520, L1
Vikhlinin, A., VanSpeybroeck, L., Markevitch, M., Forman, W. R., & Grego, L. 2002, ApJ, 578, L107
Vikhlinin, A., Voevodkin, A., Mullis, C., VanSpeybroeck, L., Quintana, H., McNamara, B., Gioia, I., Hornstrup, A., Henry, J., Forman, W., & Jones, J. 2003, ApJ, submitted, 1, 1
Voges, W. 1992, Proceedings of Satellite Symposium 3, EAS ISY-3, 9
Weinberg, S. 1972, Gravitation and Cosmology: Principles and Applications of the General Theory of Relativity (New York: John Wiley & Sons)
White, D. A., Jones, C., & Forman, W. 1997, MNRAS, 292, 419
Wu, X., Chiueh, T., Fang, L., & Xue, Y. 1998, MNRAS, 301, 861

TABLE 1
X-RAY SELECTED CLUSTER SURVEYS

Acronym	Name	Reference
160SD	160 Square Degree *ROSAT* Cluster Survey	Vikhlinin et al. 1998a; this paper
BCS+eBCS	Brightest Cluster Sample + Extended Brightest Cluster Sample	Ebeling et al. 1998, 2000
BMW-HRI	Brera Multiscale Wavelet *ROSAT* HRI Cluster Survey	Moretti et al. 2001; Panzera et al. 2003
BSHARC	Bright Serendipitous High-Redshift Archival *ROSAT* Cluster Survey	Romer et al. 2000
CIZA	Clusters in the Zone of Avoidance Survey	Ebeling, Mullis, & Tully 2002
EMSS	*Einstein* Extended Medium Sensitivity Survey	Gioia et al. 1990; Henry et al. 1992
MACS	Massive Cluster Survey	Ebeling, Edge, & Henry 2001
NEP	*ROSAT* North Ecliptic Pole Survey	Henry et al. 2001; Mullis 2001
NORAS	Northern *ROSAT* All-Sky Galaxy Cluster Survey	Böhringer et al. 2000
RASS1BS	RASS1 Bright Sample	De Grandi et al. 1999
RDCS	*ROSAT* Distant Cluster Survey	Rosati et al. 1995, 1998
REFLEX	*ROSAT*-ESO Flux Limited X-ray Galaxy Cluster Survey	Böhringer et al. 2001
RIXOS	*ROSAT* International X-ray/Optical Survey	Castander et al. 1995; Mason et al. 2000
RBS	*ROSAT* Bright Survey	Schwope et al. 2000
ROXS	*ROSAT* Optical X-Ray Survey	Donahue et al. 2001, 2002
SGP	*ROSAT* South Galactic Pole Survey	Cruddace et al. 2002, 2003
SSHARC	Southern Serendipitous High-Redshift Archival *ROSAT* Cluster Survey	Burke et al. 2003
WARPS	Wide Angle *ROSAT* Pointed Survey	Scharf et al. 1997; Perlman et al. 2002

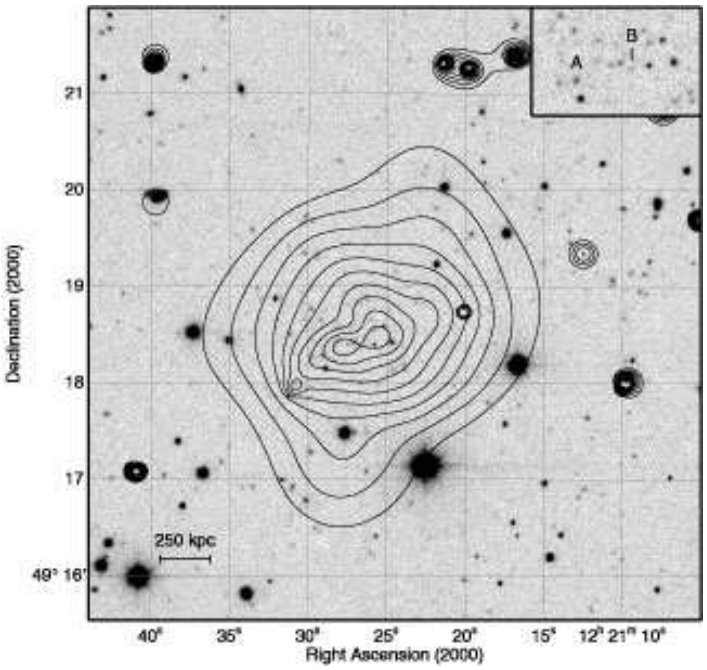

FIG. 1.— RX J1221.4+4918 (#119): a distant cluster at $z = 0.700$. A 5 minute R-band image taken with the FLWO 1.2m on 25 Jan 1998 is overlaid with adaptively smoothed X-ray flux contours in the 0.7–2.0 keV band from an 80 ks observation with the *Chandra* ACIS-I. Contours are logarithmically spaced by factors of 1.4 with the lowest contour a factor of 2 above the background (5.5×10^{-4} counts s^{-1} arcmin^2). Features in the X-ray contours are significant at a level of $\gtrsim 4\sigma$. The inset (upper-right) indicates the cluster galaxies for which redshifts were measured (see spectra in Figure 2). The R-band magnitude of galaxy A is 20.23. The scale bar shows the angular size of 250 kpc at $z = 0.700$.

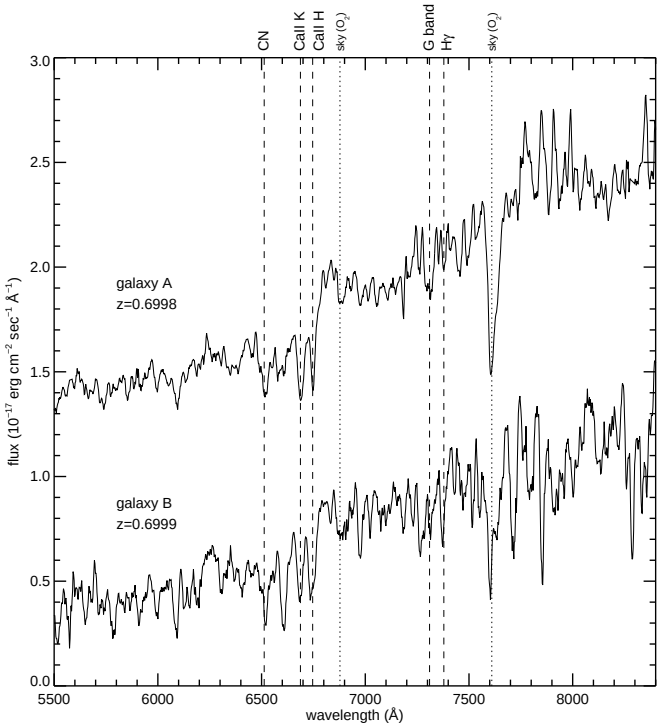

FIG. 2.— RX J1221.4+4918 (#119): a distant cluster at $z = 0.700$. Longslit spectra of galaxies A and B measured with Keck-II LRIS on 08 Jul 1999. Total integration time was 30 minutes. Galaxy A is vertically displaced by 1×10^{-17} and galaxy B is scaled by a factor of 2 for an optimal comparison of the spectra. The measured redshifts are $z_A = 0.6998 \pm 0.0004$ and $z_B = 0.6999 \pm 0.0008$. The dashed lines indicate the positions of stellar absorption features at the cluster redshift ($z = 0.700$) and the dotted lines mark the wavelengths of atmospheric absorption bands.

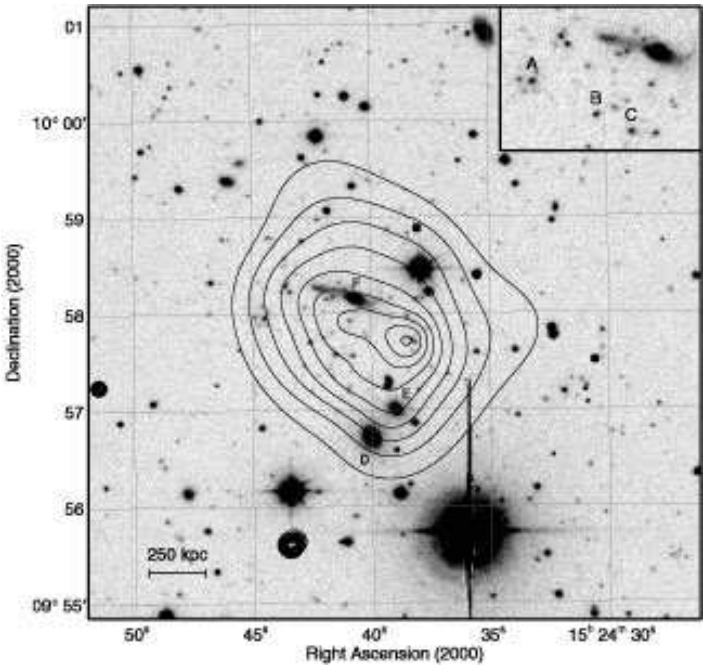

FIG. 3.— RX J1524.6+0957 (#170): a nearby group ($z = 0.078$) and a distant cluster ($z = 0.516$). A 10 minute I-band image taken with the FLWO 1.2m on 08 Jul 1997 is overlaid with adaptively smoothed X-ray flux contours in the 0.7–2.0 keV band from a 51 ks observation with the *Chandra* ACIS-I. Contours are logarithmically spaced by factors of 1.4 with the lowest contour a factor of 2 above the background (9.7×10^{-4} counts s^{-1} arcmin^2). Features in the X-ray contours are significant at a level of $\gtrsim 4\sigma$. The inset (upper-right) indicates the galaxies (A–C) of the distant cluster for which redshifts were measured (see spectra in Figure 4). The foreground group galaxies (D–F) are at redshifts $z_{\rm D} = 0.0787 \pm 0.0009$, $z_{\rm E} = 0.0767 \pm 0.0009$, and $z_{\rm F} = 0.08$? (K. Romer, priv. comm.). The R-band magnitude of galaxy C is 20.29. The scale bar shows the angular size of 250 kpc at $z = 0.516$.

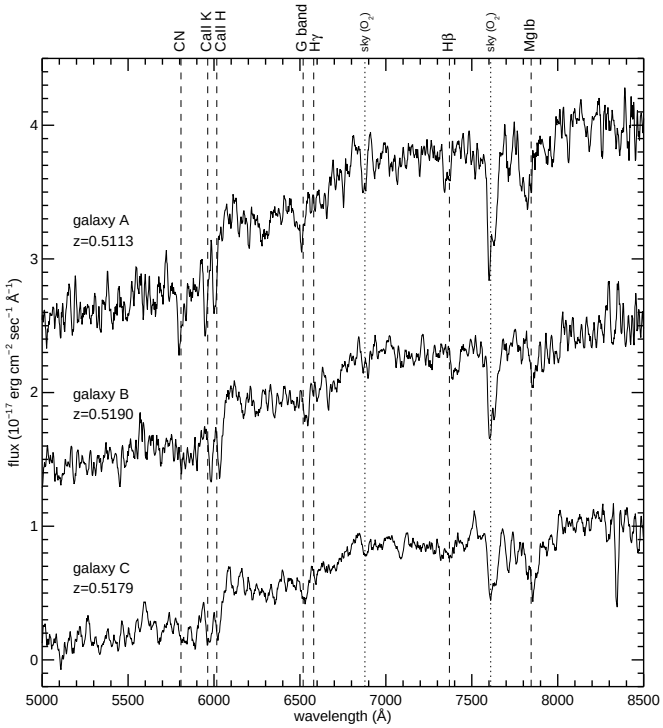

FIG. 4.— RX J1524.6+0957 (#170): a nearby group ($z = 0.078$) and a distant cluster ($z = 0.516$). Longslit spectra of galaxies A, B, and C measured with Keck-II LRIS on 27 Jan 2000. Total integration time was 20 minutes. Galaxies A and B are vertically displaced by 2×10^{-17} and 1×10^{-17}, respectively, for an optimal comparison of the spectra. The measured redshifts are $z_{\rm A} = 0.5113 \pm 0.0002$, $z_{\rm B} = 0.5190 \pm 0.0005$ and $z_{\rm C} = 0.5179 \pm 0.0004$. The dashed lines indicate the positions of stellar absorption features at the cluster redshift ($z = 0.516$) and the dotted lines mark the wavelengths of atmospheric absorption bands.

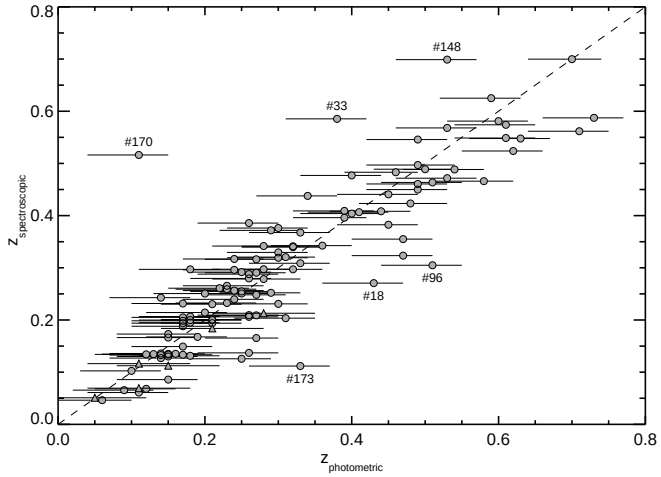

FIG. 5.— Spectroscopic redshift versus photometric redshift for the 124 clusters of the 160SD sample originally published with photometric redshifts in V98. The circles represent the 117 objects for which the photometric redshift estimates were based on CCD imaging; whereas the triangles represent the 7 objects for which photometric redshifts were based on DSS images. The horizontal error bars are the 90% confidence intervals for the photometric redshift estimates. The errors on the spectroscopic measurements are smaller than the plotting symbols. The six clusters with the largest redshift difference are labeled.

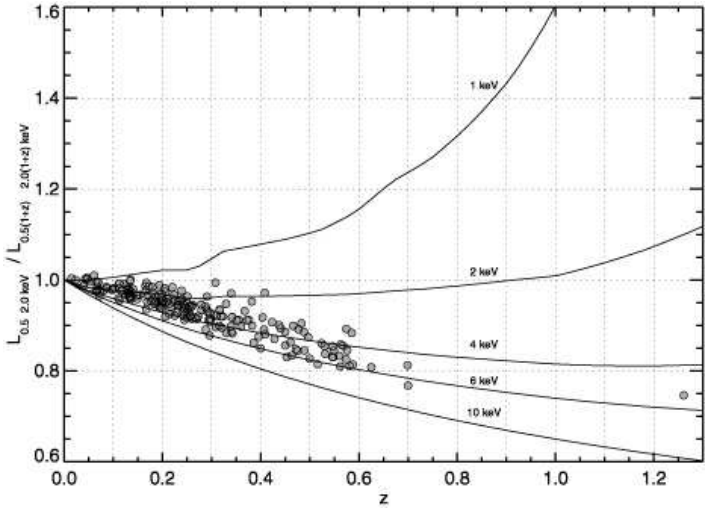

FIG. 6.— *K*-corrections as a function of redshift and ICM temperature in the 0.5 – 2.0 keV band. The model source spectrum is a Raymond-Smith plasma with a metallicity of 0.3 solar. Data points indicate the sampling of the 160SD clusters. The trend of increasing cluster temperature with increasing redshift is the result of the flux-limited nature of the survey.

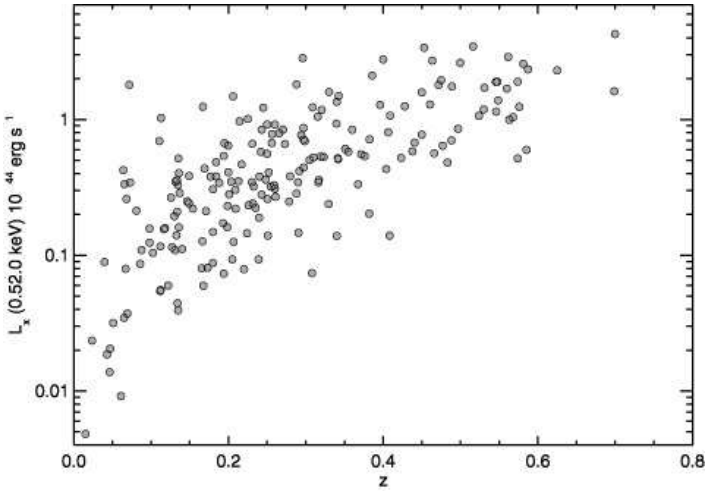

FIG. 7.— X-ray luminosity and redshift distribution of the 160SD cluster sample. The median redshift is $z_{\rm median} = 0.25$ and the median X-ray luminosity is $L_{\rm X,median} = 4.2 \times 10^{43}$ erg s^{-1}. To preserve the readability of this plot the most distant cluster (RX J0848.9+4452, $z = 1.261$, $L_{\rm X} = 2.0 \times 10^{44}$ erg s^{-1}) is not shown.

TABLE 2
OPTICAL IDENTIFICATIONS OF 160SD X-RAY SOURCES

	V98	Revised Sample (this work)
extended X-ray sources	223	223
galaxy clusters	203	201
probable false detections[a]	19	21
no follow-up observations[b]	1	1

[a]likely blends of unresolved X-ray point sources

[b]obscured by the glare of Arcturus

TABLE 3
REDSHIFTS FOR 160SD CLUSTERS

	V98	Newly Reported (this work)	Revised Sample (this work)
spectroscopic redshifts	76	124	200
measured by our group	45	110	155
literature & private comm.	31	14	45
photometric estimates	124	...	...
clusters with no redshift	3	...	1
cluster sample size	203	...	201

TABLE 4
160 SQUARE DEGREE *ROSAT* SURVEY CLUSTER CATALOG

Object Name	Number	α [J2000]	δ [J2000]	δr [″]	r_c [″]	δr_c [″]	f_X [10^{-14} cgs]	δf_X [10^{-14} cgs]	L_X [10^{44} cgs]	z	Redshift References	Notes
(1)	(2)	(3)	(4)	(5)	(6)	(7)	(8)	(9)	(10)	(11)	(12)	(13)
RX J0030.5+2618	1	00 30 33.2	+26 18 19	13	31	3	24.3	3.0	2.61	0.500		RDCS/WARPS2
RX J0041.1−2339	2	00 41 10.3	−23 39 33	19	25	12	9.8	2.4	0.06	0.112		
RX J0050.9−0929	3	00 50 59.2	−09 29 12	11	45	4	36.6	4.9	0.64	0.200		WARPS2
RX J0054.0−2823	4	00 54 02.8	−28 23 58	16	37	6	10.8	1.5	0.42	0.292		RDCS/WARP2
RX J0056.9−2213	5	00 56 55.8	−22 13 53	17	61	12	25.9	5.2	0.16	0.116		
RX J0056.9−2740	6	00 56 56.1	−27 40 12	13	14	2	6.9	0.8	1.00	0.563	1	J1888.16, RDCS
RX J0057.4−2616	7	00 57 24.2	−26 16 45	14	82	6	186.1	21.3	1.03	0.113	2	A122/REFLEX2
RX J0110.3+1938	8	01 10 18.0	+19 38 23	16	35	8	7.8	1.6	0.36	0.317		WARPS2
RX J0111.6−3811	9	01 11 36.6	−38 11 12	9	18	3	8.9	1.7	0.06	0.122		WARPS1
RX J0122.5−2832	10	01 22 35.9	−28 32 03	14	37	16	26.9	6.3	0.78	0.256		Abell S154
RX J0124.5+0400	11	01 24 35.1	+04 00 49	20	31	14	7.5	2.2	0.34	0.316		
RX J0127.4−4326	12	01 27 27.8	−43 26 13	19	34	13	5.7	1.9	F	F		F
RX J0128.6−4324	13	01 28 36.9	−43 24 57	9	10	3	7.5	1.3	0.28	0.288		
RX J0132.9−4259	14	01 32 54.7	−42 59 52	23	75	25	32.3	8.1	0.11	0.088	3	APMBGC 244–064–098
RX J0136.4−1811	15	01 36 24.2	−18 11 59	15	21	8	4.8	1.0	0.14	0.251		WARPS2
RX J0139.6+0119	16	01 39 39.5	+01 19 27	12	37	8	10.9	2.0	0.32	0.255		z_{PSPC}, RDCS/WARPS2
RX J0139.9+1810	17	01 39 54.3	+18 10 00	9	33	5	27.3	3.8	0.38	0.177	2	A227/RDCS
RX J0142.8+2025	18	01 42 50.6	+20 25 16	22	29	6	26.1	4.5	0.84	0.271		BMW
RX J0144.4+0212	19	01 44 29.1	+02 12 37	13	32	11	10.1	2.3	0.13	0.166		WARPS1
RX J0154.2−5937	20	01 54 14.8	−59 37 48	12	22	7	14.5	3.2	0.84	0.360		
RX J0159.3+0030	21	01 59 18.2	+00 30 12	9	13	2	32.7	4.1	2.11	0.386		
RX J0206.3+1511	22	02 06 23.4	+15 11 16	14	53	10	13.0	2.5	0.36	0.248		RDCS/RIXOS/WARPS1
RX J0206.8−1309	23	02 06 49.5	−13 09 04	15	28	8	26.0	4.4	1.18	0.320		
RX J0210.2−3932	24	02 10 13.8	−39 32 51	11	22	10	4.6	1.1	0.06	0.168		RDCS
RX J0210.4−3929	25	02 10 25.6	−39 29 47	14	28	9	6.4	1.3	0.08	0.165		RDCS/WARPS1
RX J0228.2−1005	26	02 28 13.2	−10 05 40	15	35	6	24.4	3.9	0.24	0.149		WARPS1
RX J0236.0−5225	27	02 36 05.2	−52 25 03	9	16	4	5.8	1.2	F	F		F
RX J0237.9−5224	28	02 37 59.2	−52 24 40	14	49	8	64.4	8.2	0.52	0.135	4	A3038/BSHARC/RDCS/REFLEX2/WARPS1
RX J0239.8−2320	29	02 39 52.6	−23 20 35	23	51	14	8.4	1.8	0.77	0.450		
RX J0258.7+0012	30	02 58 46.1	+00 12 44	19	28	7	10.8	2.9	0.33	0.259		
RX J0259.5+0013	31	02 59 33.9	+00 13 47	12	42	11	32.4	5.2	0.54	0.194		
RX J0322.3−4918	32	03 22 20.1	−49 18 40	15	69	11	40.3	7.2	0.08	0.067	5	z_{PSPC}, Abell S34
RX J0337.7−2522	33	03 37 44.9	−25 22 39	8	7	2	3.7	0.7	0.60	0.585		RDCS/SSHARC
RX J0341.9−4500	34	03 41 57.1	−45 00 11	12	27	9	1.7	0.4	0.14	0.408		RDCS
RX J0351.6−3649	35	03 51 37.8	−36 49 50	24	31	17	8.8	2.2	0.56	0.372		
RX J0428.7−3805	36	04 28 43.0	−38 05 54	20	54	13	20.8	5.0	0.22	0.154	5	A3259
RX J0434.2−0831	37	04 34 15.7	−08 31 17	24	25	14	7.2	2.2	0.19	0.240		
RX J0505.9−2825	38	05 05 57.8	−28 25 47	15	25	4	14.2	1.9	0.11	0.131		RDCS/SSHARC
RX J0506.0−2840	39	05 06 03.7	−28 40 44	21	84	20	19.5	3.4	0.16	0.136		
RX J0521.1−2530	40	05 21 10.7	−25 30 44	15	37	13	17.6	4.0	2.57	0.581		
RX J0522.2−3625	41	05 22 14.2	−36 25 04	9	16	5	18.4	3.8	1.79	0.472		BMW
RX J0528.6−3251	42	05 28 40.3	−32 51 38	8	26	3	19.9	2.5	0.66	0.273		RDCS/WARPS2
RX J0529.6−5848	43	05 29 38.4	−58 48 10	9	10	3	5.6	1.0	0.56	0.466		
RX J0532.7−4614	44	05 32 43.7	−46 14 11	7	12	1	41.1	4.3	0.33	0.135		
RX J0533.8−5746	45	05 33 53.2	−57 46 52	37	81	28	22.2	6.1	0.87	0.297		
RX J0533.9−5809	46	05 33 55.9	−58 09 16	30	53	20	9.0	2.8	0.16	0.198		
RX J0810.3+4216	47	08 10 23.9	+42 16 24	14	59	5	238.6	27.2	0.42	0.064		
RX J0818.9+5654	48	08 18 57.8	+56 54 34	17	29	9	10.1	2.5	0.31	0.260		
RX J0819.3+7054	49	08 19 22.6	+70 54 48	15	24	6	10.1	1.8	0.23	0.226		WARPS2
RX J0819.9+5634	50	08 19 54.4	+56 34 35	14	16	5	30.8	5.0	0.92	0.260		
RX J0820.4+5645	51	08 20 26.4	+56 45 22	18	39	14	22.9	4.2	0.02	0.043		
RX J0826.1+2625	52	08 26 06.4	+26 25 47	22	59	19	10.9	2.6	0.61	0.351		
RX J0826.4+3125	53	08 26 29.7	+31 25 15	31	47	22	11.1	4.7	0.22	0.209		
RX J0831.2+4905	54	08 31 16.0	+49 05 06	17	30	15	12.3	4.0	F	F		F
RX J0834.4+1933	55	08 34 27.4	+19 33 24	18	31	7	8.3	1.7	F	F		F
RX J0841.1+6422	56	08 41 07.4	+64 22 43	8	35	3	29.1	3.2	1.49	0.342		RDCS
RX J0841.7+7046	57	08 41 43.4	+70 46 53	13	31	12	8.9	2.1	0.22	0.235		
RX J0842.8+5023	58	08 42 52.8	+50 23 16	16	23	10	6.3	1.7	0.52	0.423		
RX J0847.1+3449	59	08 47 11.3	+34 49 16	17	28	9	12.2	3.0	1.69	0.560		

TABLE 4—*Continued*

Object Name	Number	α [J2000]	δ [J2000]	δr [″]	r_c [″]	δr_c [″]	f_X [10^{-14} cgs]	δf_X [10^{-14} cgs]	L_X [10^{44} cgs]	z	Redshift References	Notes
(1)	(2)	(3)	(4)	(5)	(6)	(7)	(8)	(9)	(10)	(11)	(12)	(13)
RX J0848.7+4456	60	08 48 47.6	+44 56 21	13	14	4	3.3	0.6	0.52	0.574		RDCS/WARPS2
RX J0848.9+4452	61	08 48 56.3	+44 52 16	14	23	6	2.7	0.6	1.99	1.261	6	RDCS
RX J0849.1+3731	62	08 49 11.1	+37 31 25	14	36	10	14.7	3.0	0.38	0.240		BSHARC/RIXOS/WARPS2
RX J0852.5+1618	63	08 52 33.6	+16 18 08	19	33	10	37.1	6.2	0.16	0.098		
RX J0853.2+5759	64	08 53 14.1	+57 59 39	17	35	14	19.8	5.8	1.95	0.475		
RX J0857.7+2747	65	08 57 45.7	+27 47 32	27	42	11	6.8	1.6	F	F		F
RX J0858.4+1357	66	08 58 25.0	+13 57 16	10	14	5	6.4	1.0	0.70	0.488		cluster + AGN($z = 0.494$) SSHARC/WARPS2
RX J0907.2+3330	67	09 07 17.9	+33 30 09	14	24	5	4.4	0.8	0.48	0.483		RDCS
RX J0907.3+1639	68	09 07 20.4	+16 39 09	9	55	5	148.5	17.6	0.34	0.073	7	A744/eBCS/EMSS
RX J0910.6+4248	69	09 10 39.7	+42 48 41	24	76	23	8.3	2.0	1.24	0.576	8	RDCS
RX J0921.2+4528	70	09 21 13.4	+45 28 50	11	26	5	23.9	4.7	1.05	0.315		lenses $z = 1.66$ QSO, see § 2.3
RX J0926.6+1242	71	09 26 36.6	+12 42 56	9	16	3	16.7	2.1	1.75	0.489		
RX J0926.7+1234	72	09 26 45.6	+12 34 07	41	60	22	11.7	3.5	F	F		F
RX J0943.5+1640	73	09 43 32.2	+16 40 02	10	36	5	23.1	3.7	0.67	0.256		RIXOS/WARPS2
RX J0943.7+1644	74	09 43 44.7	+16 44 20	17	69	13	21.2	4.1	0.31	0.180		RIXOS/WARPS24
RX J0947.7+0741	75	09 47 45.8	+07 41 18	17	32	10	13.5	3.7	2.30	0.625		(BSHARC/SSHARC QSO $z \sim 0.63$)
RX J0951.7−0128	76	09 51 47.0	−01 28 33	22	25	11	7.1	1.9	1.04	0.568	9	WARPS1
RX J0952.1−0148	77	09 52 08.7	−01 48 18	18	39	14	9.3	2.5	F	F		F
RX J0953.5+4758	78	09 53 31.2	+47 58 57	20	41	20	13.0	5.2	F	F		F
RX J0956.0+4107	79	09 56 03.4	+41 07 14	13	13	6	15.6	3.3	2.34	0.587		
RX J0957.8+6534	80	09 57 53.2	+65 34 30	12	19	5	9.4	1.7	1.19	0.530		
RX J0958.2+5516	81	09 58 13.5	+55 16 01	15	67	14	48.2	7.1	0.97	0.214		A899
RX J0959.4+4633	82	09 59 27.7	+46 33 57	31	37	23	10.5	5.2	F	F		F
RX J1002.6−0808	83	10 02 40.4	−08 08 46	12	29	7	8.6	2.1	1.07	0.524	10	WARPS2
RX J1010.2+5430	84	10 10 14.7	+54 30 18	14	20	4	21.0	2.9	0.02	0.047	11	RDCS/RIXOS/WARPS2
RX J1011.0+5339	85	10 11 05.1	+53 39 27	11	23	9	4.7	1.2	0.24	0.329		WARPS2
RX J1011.4+5450	86	10 11 26.0	+54 50 08	24	94	22	20.0	5.1	0.77	0.294		RDCS/RIXOS/WARPS2
RX J1013.6+4933	87	10 13 38.4	+49 33 07	22	107	21	45.6	9.8	0.36	0.133		
RX J1015.1+4931	88	10 15 08.5	+49 31 32	10	14	8	10.8	2.6	0.71	0.383		
RX J1033.8+5703	89	10 33 51.9	+57 03 10	16	24	9	14.5	4.3	0.01	0.046	12	
RX J1036.1+5713	90	10 36 11.3	+57 13 31	13	15	6	18.8	3.9	0.35	0.203		
RX J1048.0−1124	91	10 48 00.1	−11 24 07	19	35	7	18.5	3.6	0.03	0.065		
RX J1049.0+5424	92	10 49 02.7	+54 24 00	12	22	9	9.1	1.6	0.26	0.251		RIXOS
RX J1053.3+5720	93	10 53 18.4	+57 20 47	8	12	3	2.5	0.3	0.14	0.340	13	
RX J1056.2+4933	94	10 56 12.6	+49 33 11	23	64	15	12.9	1.9	0.23	0.199		RIXOS/WARPS2
RX J1058.2+0136	95	10 58 13.0	+01 36 57	15	113	13	129.5	19.3	0.09	0.040	14	A1139/eBCS/REFLEX1
RX J1117.2+1744	96	11 17 12.0	+17 44 24	26	65	33	12.0	5.6	0.50	0.305		
RX J1117.4+0743	97	11 17 26.1	+07 43 35	12	18	7	6.1	1.6	0.64	0.477		WARPS2
RX J1117.5+1744	98	11 17 30.2	+17 44 44	16	36	10	14.4	2.5	1.90	0.548		
RX J1119.7+2126	99	11 19 43.5	+21 26 44	9	12	3	5.5	0.9	0.01	0.061	11	RDCS/RIXOS/WARPS2
RX J1120.9+2326	100	11 20 57.9	+23 26 41	16	29	8	21.3	5.0	2.89	0.562		
RX J1123.1+1409	101	11 23 10.2	+14 09 44	27	49	24	18.2	4.9	0.93	0.340		
RX J1124.0−1700	102	11 24 03.8	−17 00 11	22	34	19	10.8	3.4	0.81	0.407		
RX J1124.6+4155	103	11 24 36.9	+41 55 59	31	110	30	40.1	9.6	0.67	0.195		
RX J1135.9+2131	104	11 35 54.5	+21 31 05	17	72	20	17.8	4.0	0.14	0.133		
RX J1138.7+0315	105	11 38 43.9	+03 15 38	10	18	6	15.9	3.7	0.11	0.127		
RX J1142.0+2144	106	11 42 04.6	+21 44 57	26	56	34	45.9	17.4	0.35	0.131		
RX J1146.4+2854	107	11 46 26.9	+28 54 15	18	79	11	39.2	5.8	0.38	0.149		WARPS2
RX J1151.6+8104	108	11 51 40.3	+81 04 38	14	27	7	3.7	1.1	0.15	0.290		
RX J1158.1+5521	109	11 58 11.7	+55 21 45	9	21	5	4.7	1.0	0.04	0.135		
RX J1159.8+5531	110	11 59 51.2	+55 31 56	7	24	2	74.2	7.6	0.21	0.081	15	OLEG/EMSS/RDCS/RIXOS
RX J1200.8−0327	111	12 00 49.7	−03 27 31	10	29	5	18.5	2.6	1.28	0.396		RIXOS/SSHARC/WARPS2
RX J1204.0+2807	112	12 04 04.0	+28 07 08	7	32	3	102.6	11.4	1.24	0.167	15	$z_{\rm PSPC}$, A1455/BSHARC/EMSS/NORAS/RDCS/RIXOS
RX J1204.3−0350	113	12 04 22.9	−03 50 55	14	26	6	8.7	1.3	0.27	0.261		RDCS/SSHARC/WARPS2
RX J1206.5−0744	114	12 06 33.5	−07 44 28	15	64	7	129.0	16.3	0.26	0.068		REFLEX2
RX J1211.2+3911	115	12 11 15.3	+39 11 38	8	14	4	26.6	3.8	1.35	0.340	15	BMW/BSHARC/EMSS/WARPS2
RX J1213.5+0253	116	12 13 35.3	+02 53 26	13	27	9	14.3	3.0	1.07	0.409		
RX J1216.3+2633	117	12 16 19.4	+26 33 26	15	15	6	15.4	4.2	1.25	0.428		
RX J1218.4+3011	118	12 18 29.1	+30 11 46	11	18	9	5.3	1.4	0.33	0.368		RDCS/RIXOS/WARPS2

TABLE 4—*Continued*

Object Name	Number	α	δ	δr	r_c	δr_c	f_X	δf_X	L_X	z	Redshift	Notes
		[J2000]	[J2000]	[″]	[″]	[″]	[10^{-14} cgs]	[10^{-14} cgs]	[10^{44} cgs]		References	
(1)	(2)	(3)	(4)	(5)	(6)	(7)	(8)	(9)	(10)	(11)	(12)	(13)
RX J1221.4+4918	119	12 21 24.5	+49 18 13	18	34	8	20.6	4.6	4.27	0.700		
RX J1222.5+0412	120	12 22 32.5	+04 12 02	12	15	7	6.3	1.6	F	F		F
RX J1236.5+0051	121	12 36 31.4	+00 51 43	14	28	8	4.8	1.2	0.09	0.205	12	RDCS
RX J1237.4+1141	122	12 37 25.1	+11 41 27	21	41	15	10.6	3.4	···	···		discussed in § 2.3
RX J1237.6+2632	123	12 37 38.6	+26 32 23	14	31	12	7.0	2.3	0.25	0.278		BMW
RX J1252.0−2920	124	12 52 05.4	−29 20 46	13	46	11	21.7	4.2	0.34	0.188		RDCS
RX J1252.1−2914	125	12 52 11.3	−29 14 59	8	11	5	8.7	1.6	F	F		F
RX J1254.6+2545	126	12 54 38.3	+25 45 13	13	31	7	10.2	2.0	0.17	0.193		RDCS/WARPS2
RX J1254.8+2550	127	12 54 53.6	+25 50 55	12	40	8	13.2	2.5	0.32	0.233		RDCS/WARPS2
RX J1256.0+2556	128	12 56 04.9	+25 56 52	11	30	7	9.9	1.9	0.24	0.232		RDCS/WARPS2
RX J1256.6+4715	129	12 56 39.4	+47 15 19	10	25	5	5.7	0.8	0.43	0.404	11	RDCS/RIXOS/WARPS2
RX J1301.7+1059	130	13 01 43.6	+10 59 33	18	54	11	28.1	5.6	0.66	0.231		
RX J1309.9+3222	131	13 09 55.6	+32 22 31	23	42	19	9.0	2.9	0.34	0.290		
RX J1311.2+3228	132	13 11 12.8	+32 28 58	8	22	3	46.7	5.8	1.22	0.245	15	BSHARC/EMSS/RIXOS/WARPS2
RX J1311.5−0551	133	13 11 30.2	−05 51 26	20	36	6	13.7	2.4	1.29	0.461		
RX J1325.2+6550	134	13 25 14.9	+65 50 29	28	54	21	10.1	3.1	0.15	0.180		$z_{\rm PSPC}$, WARPS2
RX J1325.7−2943	135	13 25 43.9	−29 43 51	17	43	11	7.7	2.7	F	F		F
RX J1329.4+1143	136	13 29 27.3	+11 43 31	22	120	16	97.0	16.6	0.02	0.024	16	NGC 5171 group
RX J1334.5−0822	137	13 34 31.1	−08 22 29	10	13	5	5.2	1.1	F	F		F
RX J1334.5+3756	138	13 34 34.4	+37 56 58	11	16	5	1.6	0.3	0.07	0.308	17	
RX J1335.0+3750	139	13 35 03.7	+37 50 00	9	21	4	2.9	0.4	0.20	0.382	17	RDCS
RX J1336.7+3837	140	13 36 42.1	+38 37 32	16	20	9	5.9	1.6	0.09	0.180		
RX J1337.8+4815	141	13 37 48.3	+48 15 46	10	16	4	7.1	1.5	F	F		F
RX J1337.8+2638	142	13 37 50.4	+26 38 49	12	21	6	9.6	2.1	0.51	0.342		WARPS2
RX J1337.8+3854	143	13 37 53.3	+38 54 09	17	32	9	14.3	3.6	0.41	0.252		
RX J1340.5+4017	144	13 40 33.5	+40 17 47	10	19	5	16.1	2.5	0.21	0.171	18	OLEG
RX J1340.8+3958	145	13 40 53.7	+39 58 11	19	66	16	34.4	6.9	0.44	0.169	19	A1774
RX J1341.8+2622	146	13 41 51.7	+26 22 54	8	103	4	814.0	84.6	1.80	0.072	20	A1775/BCS/NORAS/RBS
RX J1342.0+5200	147	13 42 05.0	+52 00 37	13	10	4	12.4	1.9	F	F		F
RX J1342.8+4028	148	13 42 49.1	+40 28 11	16	15	6	7.4	2.0	1.62	0.699		WARPS2
RX J1343.4+4053	149	13 43 25.0	+40 53 14	10	18	7	12.6	2.8	0.11	0.140		
RX J1343.4+5547	150	13 43 29.0	+55 47 17	23	109	17	17.5	2.8	0.04	0.069		RIXOS
RX J1354.2−0221	151	13 54 16.9	−02 21 47	11	27	4	14.5	2.6	1.89	0.546		RDCS/SSHARC
RX J1354.8+6917	152	13 54 49.1	+69 17 20	15	26	10	6.4	1.9	0.13	0.207		
RX J1406.2+2830	153	14 06 16.3	+28 30 52	9	14	4	8.5	1.2	1.14	0.546	21	RDCS/WARPS1
RX J1406.9+2834	154	14 06 54.9	+28 34 17	8	30	3	25.7	3.2	0.16	0.118	21	BMW/BSHARC/RDCS/WARPS1
RX J1410.2+5942	155	14 10 12.4	+59 42 40	18	38	12	33.5	5.1	0.92	0.250	22	probably part of A1877
RX J1410.2+5938	156	14 10 15.2	+59 38 31	17	31	22	20.1	8.7	0.56	0.250	22	probably part of A1877
RX J1415.6+1906	157	14 15 37.9	+19 06 33	13	52	5	25.4	3.4	···	···		obscured by Arcturus
RX J1416.4+4446	158	14 16 28.7	+44 46 41	8	16	4	40.4	5.2	2.77	0.400		
RX J1418.5+2510	159	14 18 31.1	+25 10 50	7	33	1	75.6	7.8	2.84	0.296	9	BMW/BSHARC/RDCS/WARPS1
RX J1418.7+0644	160	14 18 45.2	+06 44 02	9	18	5	16.4	3.0	F	F		
RX J1419.3+0638	161	14 19 23.5	+06 38 42	9	17	4	13.1	1.9	1.90	0.574	10	WARPS2
RX J1419.9+0634	162	14 19 57.2	+06 34 26	15	35	7	10.3	2.1	1.38	0.549	10	WARPS2
RX J1429.6+4234	163	14 29 38.1	+42 34 25	26	35	12	8.5	2.4	F	F		F
RX J1438.9+6423	164	14 38 55.5	+64 23 44	19	103	11	26.2	3.6	0.25	0.146		BMW
RX J1444.1+6344	165	14 44 07.7	+63 44 58	15	26	9	17.4	3.2	0.69	0.299	22	$z_{\rm PSPC}$, A1969
RX J1500.0+2233	166	15 00 02.7	+22 33 51	24	37	17	14.5	4.5	0.35	0.230		$z_{\rm PSPC}$
RX J1500.8+2244	167	15 00 51.5	+22 44 41	16	31	10	17.8	4.2	1.58	0.450		
RX J1515.5+4346	168	15 15 32.5	+43 46 39	18	60	19	34.6	9.7	0.29	0.137		
RX J1515.6+4350	169	15 15 36.8	+43 50 50	22	34	18	10.5	3.8	0.28	0.243		
RX J1524.6+0957	170	15 24 40.3	+09 57 39	9	26	3	30.4	4.1	3.45	0.516		cl + group ($z = 0.078$), BSHARC/WARPS2
RX J1537.7+1200	171	15 37 44.3	+12 00 26	30	84	26	26.4	7.4	0.21	0.134		
RX J1540.8+1445	172	15 40 53.3	+14 45 34	13	17	8	7.6	2.0	0.68	0.441		
RX J1544.0+5346	173	15 44 05.0	+53 46 27	19	35	11	9.7	2.2	0.05	0.112		
RX J1547.3+2056	174	15 47 20.7	+20 56 50	24	51	20	25.4	7.0	0.79	0.266		$z_{\rm PSPC}$
RX J1552.2+2013	175	15 52 12.3	+20 13 45	9	59	7	49.5	6.0	0.40	0.136		BSHARC/WARPS1
RX J1606.7+2329	176	16 06 42.5	+23 29 00	12	34	13	12.1	2.8	0.53	0.310		WARPS2
RX J1620.3+1723	177	16 20 22.0	+17 23 05	12	35	8	20.8	3.7	0.12	0.112		$z_{\rm PSPC}$

TABLE 4—*Continued*

Object Name	Number	α	δ	δr	r_c	δr_c	f_X	δf_X	L_X	z	Redshift	Notes
		[J2000]	[J2000]	[″]	[″]	[″]	[10^{-14} cgs]	[10^{-14} cgs]	[10^{44} cgs]		References	
(1)	(2)	(3)	(4)	(5)	(6)	(7)	(8)	(9)	(10)	(11)	(12)	(13)
RX J1629.7+2123	178	16 29 46.1	+21 23 54	19	46	8	25.3	4.0	0.38	0.184		
RX J1630.2+2434	179	16 30 15.2	+24 34 59	23	129	13	179.4	25.9	0.33	0.066		MCG +04–39–010 group
RX J1631.0+2122	180	16 31 04.6	+21 22 02	16	58	14	29.1	6.4	0.12	0.098		
RX J1633.6+5714	181	16 33 40.0	+57 14 37	14	24	8	3.5	0.7	0.09	0.239		RDCS/RIXOS/WARPS2
RX J1639.9+5347	182	16 39 55.6	+53 47 56	12	170	8	130.5	14.8	0.69	0.111	23	A2220/WARPS2
RX J1641.1+8232	183	16 41 10.0	+82 32 27	13	78	11	80.5	10.9	1.48	0.206		TTR95 1646+82 cluster, BSHARC
RX J1641.8+4001	184	16 41 52.5	+40 01 29	24	51	15	29.4	7.8	2.72	0.464		
RX J1642.5+3959	185	16 42 33.5	+39 59 05	12	19	9	5.3	1.4	F	F		F, QSO 1640+400 $z = 1.59$
RX J1642.6+3935	186	16 42 38.9	+39 35 53	16	27	9	10.1	2.3	0.58	0.355		
RX J1658.5+3430	187	16 58 34.7	+34 30 12	16	58	10	33.6	5.2	1.60	0.330		
RX J1659.7+3410	188	16 59 44.6	+34 10 17	16	25	11	9.8	3.4	0.52	0.341		
RX J1700.7+6413	189	17 00 42.3	+64 13 00	7	18	1	45.6	4.7	1.01	0.225	24	A2246/NORAS/RDCS
RX J1701.3+6414	190	17 01 23.0	+64 14 11	7	25	2	38.6	4.2	3.38	0.453		RDCS/BSHARC
RX J1701.7+6421	191	17 01 46.1	+64 21 15	14	32	8	3.5	0.7	0.08	0.220		RDCS
RX J1702.2+6420	192	17 02 13.3	+64 20 00	12	32	7	6.3	1.2	0.15	0.224		RDCS/WARPS2
RX J1722.8+4105	193	17 22 53.8	+41 05 25	22	42	12	29.4	6.5	1.23	0.309		
RX J1729.0+7440	194	17 29 01.9	+74 40 46	40	100	31	17.3	7.2	0.35	0.213		
RX J1746.4+6848	195	17 46 29.1	+68 48 54	13	56	10	22.3	3.2	0.47	0.217		RDCS/WARPS2
RX J2003.4−5556	196	20 03 28.4	−55 56 47	8	16	2	47.6	6.3	0.00	0.015	5	Abell S840
RX J2004.8−5603	197	20 04 49.4	−56 03 44	16	30	11	10.4	2.5	F	F		F
RX J2005.2−5612	198	20 05 13.6	−56 12 58	9	7	3	35.0	4.9	F	F		F
RX J2059.9−4245	199	20 59 55.2	−42 45 33	8	9	3	11.2	1.8	0.53	0.323		
RX J2108.8−0516	200	21 08 51.2	−05 16 49	12	34	7	11.6	1.7	0.53	0.319		BMW/RDCS/SSHARC/WARPS1
RX J2114.3−6800	201	21 14 20.4	−68 00 56	13	17	3	25.8	3.3	0.19	0.130	25	OLEG/RDCS/SSHARC
RX J2137.1+0026	202	21 37 06.7	+00 26 51	21	55	20	27.8	5.7	0.03	0.051	26	UGC 11780 group
RX J2139.9−4305	203	21 39 58.5	−43 05 14	15	12	6	8.3	2.0	0.54	0.376		
RX J2146.0+0423	204	21 46 04.8	+04 23 19	13	17	2	13.8	2.1	1.71	0.531		
RX J2202.7−1902	205	22 02 44.9	−19 02 10	22	36	9	6.6	2.2	0.58	0.438		RDCS/SSHARC/WARPS2
RX J2212.6−1713	206	22 12 38.2	−17 13 55	12	22	13	5.4	1.4	0.04	0.134		$z_{\rm PSPC}$
RX J2213.5−1656	207	22 13 31.0	−16 56 11	17	41	12	18.1	3.2	0.71	0.297		
RX J2239.4−0547	208	22 39 24.7	−05 47 04	13	11	2	22.2	3.5	0.58	0.242	9	A2465S/WARPS1
RX J2239.5−0600	209	22 39 34.4	−06 00 14	19	21	10	5.9	2.0	0.08	0.173		WARPS1
RX J2239.6−0543	210	22 39 38.9	−05 43 18	15	34	5	32.4	5.0	0.84	0.243	9	A2465N/WARPS1
RX J2247.4+0337	211	22 47 29.1	+03 37 13	20	46	17	23.0	6.3	0.41	0.200		OLEG
RX J2257.8+2056	212	22 57 49.4	+20 56 25	11	22	7	11.1	2.1	0.44	0.297		WARPS2
RX J2258.1+2055	213	22 58 07.1	+20 55 07	9	24	3	50.5	6.1	1.81	0.288	15	Zw2255.5+2041/BSHARC/EMSS/WARPS2
RX J2305.4−3546	214	23 05 26.2	−35 46 01	15	55	14	15.5	3.4	0.28	0.201		
RX J2305.4−5130	215	23 05 26.6	−51 30 30	17	21	10	4.2	1.4	0.07	0.194		RDCS
RX J2318.0−4235	216	23 18 04.8	−42 35 30	17	28	8	15.5	2.7	0.30	0.209		BMW
RX J2319.5+1226	217	23 19 33.9	+12 26 17	10	30	6	38.2	4.7	0.27	0.126		RIXOS/WARPS1
RX J2325.6−5443	218	23 25 39.1	−54 43 59	35	91	26	22.4	7.7	0.10	0.102		
RX J2328.8+1453	219	23 28 49.9	+14 53 12	21	27	12	7.6	1.7	0.85	0.497		WARPS2
RX J2331.8−3747	220	23 31 52.1	−37 47 11	28	46	25	10.8	4.7	0.38	0.280		
RX J2348.8−3117	221	23 48 53.7	−31 17 20	12	43	8	32.5	5.1	0.49	0.184		A4043
RX J2349.1−3122	222	23 49 07.6	−31 22 26	11	21	6	6.0	1.4	F	F		F
RX J2355.1−1500	223	23 55 11.8	−15 00 26	26	70	20	26.6	6.7	0.09	0.086		

Note. — Units of right ascension are hours, minutes, and seconds, and units of declination are degrees, arcminutes, and arcseconds. Units of X-ray flux are 10^{-14} erg cm^{-2} s^{-1} and units of X-ray luminosity are 10^{44} h$_{50}^{-2}$ erg s^{-1}, both of which are in the 0.5–2.0 keV energy band. Redshift references — (1) Couch et al. 1991; (2) Quintana & Ramirez 1995; (3) Loveday et al. 1996; (4) Nesci & Altamore 1990; (5) Abell, Corwin, & Olowin 1989; (6) Rosati et al. 1999; (7) Kurtz et al. 1985; (8) P. Rosati (private communication); (9) Perlman et al. 2002; (10) H. Ebeling (private communication); (11) Mason et al. 2000; (12) J. Huchra (private communication); (13) Schmidt et al. 1998; (14) Struble & Rood 1999; (15) Stocke et al. 1991; (16) Mahdavi et al. 2000; (17) McHardy et al. 1998; (18) Ponman et al. 1994; (19) Kopylov, Fetisova, & Shvartsman 1984; (20) Oegerle, Hill, & Fitchett 1995; (21) Boyle, Wilkes, & Elvis 1997; (22) Huchra et al. 1990; (23) Ulrich 1976; (24) Schneider, Gunn, & Hoessel 1983; (25) Griffiths et al. 1992; (26) Huchra, Vogeley, & Geller 1999. Table 4 is also available in machine-readable form in the electronic edition of the *Astrophysical Journal*.

TABLE 5
160SD CLUSTER MEMBERSHIPS IN OTHER SURVEYS

Other Survey	Coincidences with 160SD	Percentage of 160SD	Percentage of Other Survey	Sample Size of Other Survey	Parent Dataset of Other Survey
BCS	1	0.5 %	0.5 %	201	RASS
eBCS	2	1.0 %	2.0 %	99	RASS
BMW-HRI	9	4.5 %	6.0%	∼150	*ROSAT* HRI
BSHARC	12	6.0 %	32.4 %	37	*ROSAT* PSPC
CIZA	0	···	···	150	RASS
EMSS	6	3.0 %	6.7 %	89	*Einstein* IPC
MACS	0	···	···	120	RASS
NEP	0	···	···	63	RASS
NORAS	3	1.5 %	0.8 %	378	RASS
RASS1BS	0	···	···	126	RASS
RBS	1	0.5 %	0.5 %	186	RASS
RDCS	46	22.9 %	36.5 %	126	*ROSAT* PSPC
REFLEX-I	1	0.5 %	0.2 %	452	RASS
REFLEX-II	3	1.5 %	0.8 %	∼375	RASS
RIXOS	18	9.0 %	58.0 %	31	*ROSAT* PSPC
SGP	0	···	···	186	RASS
SSHARC	9	4.4 %	28.1 %	32	*ROSAT* PSPC
WARPS-I	16	8.0 %	47.1 %	34	*ROSAT* PSPC
WARPS-II	44	21.9 %	35.5 %	124	*ROSAT* PSPC